Journal of Geophysical Research: Atmospheres

RESEARCH ARTICLE
10.1029/2018JD028285

Special Section:
Simulations of Stratospheric Sulfate Aerosol Geoengineering with the Whole Atmosphere Community Climate Model (WACCM)

Stratospheric Response in the First Geoengineering Simulation Meeting Multiple Surface Climate Objectives

Jadwiga, H. Richter[1], Simone Tilmes[1,2], Anne Glanville[1,2], Ben Kravitz[3], Douglas G. MacMartin[4,5], Michael J. Mills[2], Isla R. Simpson[1], Francis Vitt[2], Joseph J. Tribbia[1], and Jean-Francois Lamarque[1]

[1]Climate and Global Dynamics Laboratory, National Center for Atmospheric Research, Boulder, CO, USA, [2]Atmospheric Chemistry, Observations, and Modeling Laboratory, National Center for Atmospheric Research, Boulder, CO, USA, [3]Pacific Northwest National Laboratory, Richland, WA, USA, [4]Mechanical and Aerospace Engineering, Cornell University, Ithaca, NY, USA, [5]Department of Computing and Mathematical Sciences, California Institute of Technology, Pasadena, CA, USA

Abstract We describe here changes in stratospheric dynamics and chemistry in a first century-long sulfate aerosol geoengineering simulation in which the mean surface temperature and the interhemispheric and equator-to-pole surface temperature gradients were kept near their 2020 levels despite the RCP8.5 emission scenario. Simulations were carried out with the Community Earth System Model, version 1 with the Whole Atmosphere Community Climate Model as its atmospheric component [CESM1(WACCM)] coupled to a feedback algorithm controlling the magnitude of sulfur dioxide (SO_2) injections at four injection latitudes. We find that, throughout the entire geoengineering simulation, the lower stratospheric temperatures increase by ~0.19 K per Tg SO_2 injection per year or ~10 K with ~40 Tg SO_2/year total SO_2 injection. These temperature changes are associated with a strengthening of the polar jets in the stratosphere and weakening of the mean zonal wind in the lower stratosphere subtropics and throughout the troposphere, associated with weaker storm track activity. In the geoengineering simulation the quasi-biennial oscillation of the tropical lower stratospheric winds remains close to the presently observed quasi-biennial oscillation, even for large amounts of SO_2 injection. Water vapor in the stratosphere increases substantially: by 25% with ~20 Tg SO_2/year annual injection and by up to 90% with a ~40 Tg SO_2/year injection. Stratospheric column ozone in the geoengineering simulation is predicted to recover to or supersede preozone hole conditions by the end of the century.

Key Points:
- Stratospheric dynamics and chemistry are examined in a geoengineering simulation in which three surface temperature goals are met
- Stratospheric extratropical winds increase, subtropical jets and storm tracks weaken, frequency of SSWs is reduced, QBO similar to present
- Stratospheric water vapor increases, column ozone increases to preozone hole levels by the end of century, ozone hole recovery is delayed

Supporting Information:
- Supporting Information S1

Correspondence to:
J. H. Richter,
jrichter@ucar.edu

Citation:
Richter, J. H., Tilmes, S., Glanville, A., Kravitz, B., MacMartin, D. G., Mills, M. J., et al. (2018). Stratospheric response in the first geoengineering simulation meeting multiple surface climate objectives. *Journal of Geophysical Research: Atmospheres*, *123*. https://doi.org/10.1029/2018JD028285

Received 5 JAN 2018
Accepted 24 APR 2018
Accepted article online 9 MAY 2018

1. Introduction

Geoengineering is a deliberate modification of the Earth's climate proposed in order to counteract some of the effects of global warming. Perhaps the most studied method of geoengineering is the injection of sulfur dioxide (SO_2) into the stratosphere, which increases the burden of stratospheric sulfate aerosols and hence the Earth's albedo (Crutzen, 2006; National Research Council, 2015). Numerous modeling studies have demonstrated the ability of enhanced stratospheric sulfate aerosols to reflect a portion of incoming shortwave (SW) radiation and consequently to decrease Earth's global mean surface temperature (e.g., English et al., 2012; Rasch et al., 2008; Tilmes et al., 2009). These studies have been carried out either with fixed sulfate aerosol distributions or continuous SO_2 injections at specific locations or via global solar reductions performed in many past studies such as those carried out as part of the Geoengineering Model Intercomparison project (GeoMIP; Kravitz et al., 2011). These studies found that solar radiation management imperfectly compensates for the effects of increased carbon dioxide, resulting in side effects on other aspects of Earth's climate. In particular, while many studies have shown that using global solar reduction to restore global mean temperatures is quite effective at offsetting changes due to CO_2, there are some side effects. These include overcooling of the tropics and not entirely alleviating the warming of the poles (e.g., Kravitz et al., 2013; Schmidt et al., 2012), as well as changes to the hydrological cycle (e.g., Tilmes et al., 2013) and extreme events (Curry et al., 2014).

In addition, stratospheric aerosol geoengineering would affect the mean climate of the stratosphere. In particular, sulfate aerosols absorb shortwave and longwave radiation (Ferraro et al., 2011), and hence heat the

stratosphere and alter stratospheric dynamics (Richter et al., 2017; Stenchikov et al., 2002; Tilmes et al., 2009, 2018). Richter et al. (2017) showed that independent of injection latitude between 30°S and 30°N, the maximum stratospheric warming always occurs in the tropics. This is related to the temperature response being directly affected by aerosol heating but also by dynamical heating and feedbacks.

Modeling studies suggest that warming of the tropical lower stratosphere could lead to strengthening of the polar vortex (Driscoll et al., 2012; Ferraro et al., 2015; Tilmes et al., 2009, 2018) as well as changes in the tropospheric tropical circulation (Ferraro et al., 2015). The most pronounced change in stratospheric winds in these modeling studies due to modified stratospheric aerosols occurs in the tropics. The quasi-biennial oscillation (QBO) is an oscillation of the lower stratospheric tropical zonal mean zonal wind with a mean period of 28 months. Injections of SO_2 into the tropical stratosphere in general circulation models have been shown to lengthen the period of the QBO (Jones et al., 2016; Richter et al., 2017) and cause it to completely disappear at higher injection rates (Aquila et al., 2014; Niemeier & Schmidt, 2017). Richter et al. (2017) also showed that the QBO period decreases from 24 to 12–17 months in simulations with SO_2 injections at 15°S/15°N and 30°S/30°N latitude (instead of at the equator, as is often done in geoengineering simulations).

The modeled effects of SO_2 injection on stratospheric circulation depend on the amount and distribution of stratospheric aerosols as well as on the atmospheric processes considered. The distribution of aerosols in the stratosphere depends on several processes. After injections into the stratosphere, aerosols are distributed throughout the stratosphere by the Brewer Dobson Circulation (BDC) and mixing (Butchart, 2014). The deep branch of the BDC moves aerosols upward in the so-called "tropical pipe" (Plumb, 1996) and then poleward and downward. The shallow branches of the BDC move aerosols primarily latitudinally, closer to the tropopause. Mixing in the stratosphere occurs primarily over the midlatitude jets (up to 25 km), in the region of planetary wave breaking, often referred to as the "surf zone." Horizontal transport is impeded in regions of sharp gradients of potential vorticity, such as near the polar vortex in the winter months, or in the tropics near regions of the QBO (e.g., Trepte & Hitchman, 1992). The transport of aerosols for various stratospheric SO_2 injection locations and their resulting distributions in different seasons was discussed in detail in Tilmes et al. (2017) and Niemeier and Schmidt (2017).

Modeling studies have shown that modification of stratospheric aerosols also change stratospheric chemistry, including water vapor and ozone. Heckendorn et al. (2009) and Tilmes et al. (2018) showed that the heating of the tropical cold point tropopause increases stratospheric water vapor. The increase in stratospheric water vapor also contributes to enhanced ozone depletion, especially in high northern latitudes (Tilmes et al., 2018). Tilmes et al. (2009) and Pitari et al. (2014) also showed that geoengineering with sulfate aerosols results in a decrease in the ozone layer in middle and high latitudes, and Tilmes et al. (2012) demonstrated significant impact on surface ultraviolet (UV) radiation; however, Pitari et al. (2014) did not.

The majority of the above described modeling studies have focused on examining the effects of geoengineering using a prescribed stratospheric aerosol distribution or injection of SO_2 into the stratosphere with fixed amount and location and examining the climate impacts. In recent years, several novel studies have asked the question whether it is possible to design geoengineering to meet specific climate goals (Ban-Weiss & Caldeira, 2010; MacMartin et al., 2013). The first successful demonstration in a climate model of meeting specified global mean temperature objectives by modulating the amount of solar irradiance reduction using feedback was performed by MacMartin et al. (2014). Kravitz et al. (2016) then demonstrated using two distinct climate models that a feedback algorithm can be used to change solar irradiance in latitude-dependent patterns and achieve three global temperature objectives. Recently, Kravitz et al. (2017) described a first simulation with sulfate aerosol geoengineering designed to meet multiple simultaneous surface climate objectives. For this, a state-of-the art climate model, Community Earth System Model, version 1 with the Whole Atmosphere Community Climate Model [CESM1(WACCM)], was coupled to a feedback control algorithm to determine the injection amount at four predefined latitudes. It was demonstrated that it is possible to keep the mean surface temperature, the interhemispheric surface temperature gradient, and the equator-to-pole surface temperature gradient near 2020 levels using interactive SO_2 injections in a sophisticated model, which includes comprehensive chemical and dynamical coupling. As shown by Kravitz et al. (2017), the amount of SO_2 injected into the stratosphere to offset RCP8.5 conditions after 2020 reaches ~50 Tg SO_2/year by the year 2099. Such large injections of SO_2 into the stratosphere have consequences for the dynamics and the chemistry of the upper troposphere and stratosphere that need to be understood. In this work we explore these changes in stratospheric and tropospheric dynamics and stratospheric chemistry, presenting a whole atmosphere

perspective of the geoengineering strategy described in Kravitz et al. (2017). This manuscript is organized as follows: Section 2 summarizes the modeling framework and simulation details. Section 3 presents the results focusing on differences in dynamics and chemistry in the stratosphere between the RCP8.5 and feedback simulations. Section 4 presents summary and conclusions.

2. Model and Simulation Details

2.1. Model Description

The simulations presented here were carried out with CESM1(WACCM), a fully coupled Earth system model, coupling atmospheric, ocean, land, and sea-ice components. The atmospheric component of CESM1(WACCM) used here has a horizontal resolution of 0.95° latitude and 1.25° longitude, 70 vertical layers, and a model top near 140 km. Atmospheric physics is based on the Community Atmosphere Model, version 5 (CAM5; Neale et al., 2012). The nonorographic gravity wave parameterization follows the formulation used in CESM1(WACCM) with 1.9°| × 2.5° horizontal resolution described in Mills et al. (2016) but with parameter modifications for the model's horizontal resolution. The 0.95° × 1.25° CESM1(WACCM) used in this study is able to simulate the QBO (Mills et al., 2017). The QBO in CESM1(WACCM) is primarily driven by large-scale Kelvin and mixed-Rossby gravity waves, which are resolved in the model and by parameterized mesoscale waves generated by convection. In CESM1(WACCM), the properties of convectively generated gravity waves are coupled to the properties of convection (Mills et al., 2017; Richter et al., 2010). More specifically, the convective heating depth determines the range of phase speeds of gravity waves, and the amplitude of momentum flux is proportional to the square of the amplitude of convective heating (Beres et al., 2004, 2005).

CESM1(WACCM) uses a fully interactive stratospheric chemistry formulation based on the Model for OZone And Related chemical Tracers, MOZART3 (Kinnison et al., 2007). It includes a modal aerosol treatment, including sulfate, following the three-mode version of the Modal Aerosol Model (MAM3) (Liu et al., 2012). MAM3 is coupled to the microphysics as described by Mills et al. (2016). The version of CESM1(WACCM) used in this study was validated against observations for studies of sulfate aerosol injection by Mills et al. (2017) and was used in several related studies of SO_2 injection into the stratosphere (Kravitz et al., 2017; MacMartin et al., 2017; Richter et al., 2017; Tilmes et al., 2017).

2.2. Simulation Details

We examine two simulations with CESM1(WACCM). First is the reference or RCP8.5 simulation (without geoengineering), which started in 1975 as a climate validation simulation described by Mills et al. (2017) and was extended until year 2100 following the RCP8.5 scenario (Meinshausen et al., 2011). The second simulation is the geoengineering with feedback (or simply "feedback") simulation, which uses SO_2 injections at multiple locations to maintain three climate objectives: (1) global mean surface temperature (T_0), (2) the interhemispheric surface temperature gradient (T_1), and (3) the equator-to-pole gradient (T_2) near 2020 values, or more precisely at an average of these quantities between 2015 and 2024 in the RCP8.5 simulation. SO_2 injections are continuously placed in the stratosphere at four locations: 15°S/15°N at ~25 km and 30°S and 30°N at ~23 km. The amount of SO_2 injection at each location is independently adjusted annually by a feedback algorithm. At the beginning of each simulation year, the feedback algorithm decides where and how much injection should occur, based on differences from the temperature targets over past years. The algorithm was developed using detailed sensitivity studies of the climate response to various SO_2 injections at one or multiple locations (MacMartin et al., 2017; Tilmes et al., 2017). Kravitz et al. (2017) demonstrated that the feedback simulation presented here succeeded at meeting three surface climate goals, keeping T_0, T_1, and T_2 near 2020 levels. More details on the feedback algorithm, and surface climate changes in this simulation can be found in Kravitz et al. (2017), and the details of how one might determine such an algorithm are provided by Kravitz et al. (2016). The amount of SO_2 chosen by the feedback algorithm and injected every year is shown in the bottom panel of Figure 2 of Kravitz et al. (2017). This figure is repeated here in Figure 1.

3. Results

3.1. Aerosol Distribution

As shown in Kravitz et al. (2017), in the geoengineering with feedback simulation, between 2020 and 2040, SO_2 injections occur primarily at 30°S, 15°S, and 30°N, with a total of ~12 Tg SO_2/year by 2040 (Figure 1). Such SO_2 injections result in an SO_4 distribution that is primarily concentrated in the Tropics, with a maximum between 15° and 30°S, as shown in Figure 2a. After 2040, SO_2 was injected in approximately equal amounts at 30°S and 30°N, increasing linearly up to 22 Tg SO_2/year at each location by year 2100 (Figure 1). A small fraction

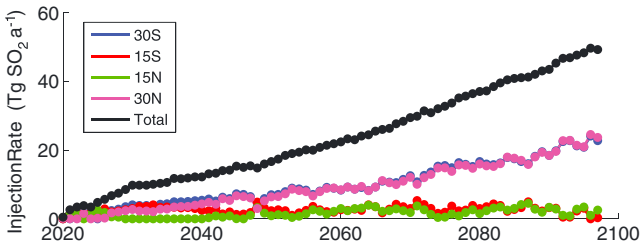

Figure 1. Injection rate of SO_2 in Tg SO_2 per year for the feedback simulation at 30°S (blue circles), 15°S (red circles), 15°N (green circles), 30°N (magenta circles), and total (black circles). Adapted with permission from Kravitz et al., 2017.

of the total SO_2, up to 5 Tg S/year, was injected at 15°S and 15°N from 2040 to 2100. As discussed by Tilmes et al. (2017), SO_2 injected at 15°S and 15°N is primarily transported by the upper branch of the BDC upward and toward the polar region. Aerosols formed from injections at 30°S and 30°N are transported primarily by horizontal mixing and the shallow branch of the BDC horizontally toward the polar regions (Niemeier & Schmidt, 2017; Tilmes et al., 2017). By the time period from 2060 to 2079 stratospheric SO_4 mixing ratios in the geoengineering simulation reach 50 μg S/kg air, which is 2 orders of magnitude greater than the peak background tropospheric (or stratospheric) SO_4 mixing ratio found in the RCP8.5 simulation (not shown). By the time period from 2080 to 2099, the annual SO_2 injection into the stratosphere is approximately 4 times what Mount Pinatubo injected into the stratosphere and the annual stratospheric SO_4 mixing ratio reaches over 70 μg S/kg air near 25°S/25°N and 30 hPa. That mixing ratio is over 3 times the maximum stratospheric SO_4 mixing ratio in the year 1992 (annual average) after the Mount Pinatubo eruption (Figure 3). By 2080–2099,

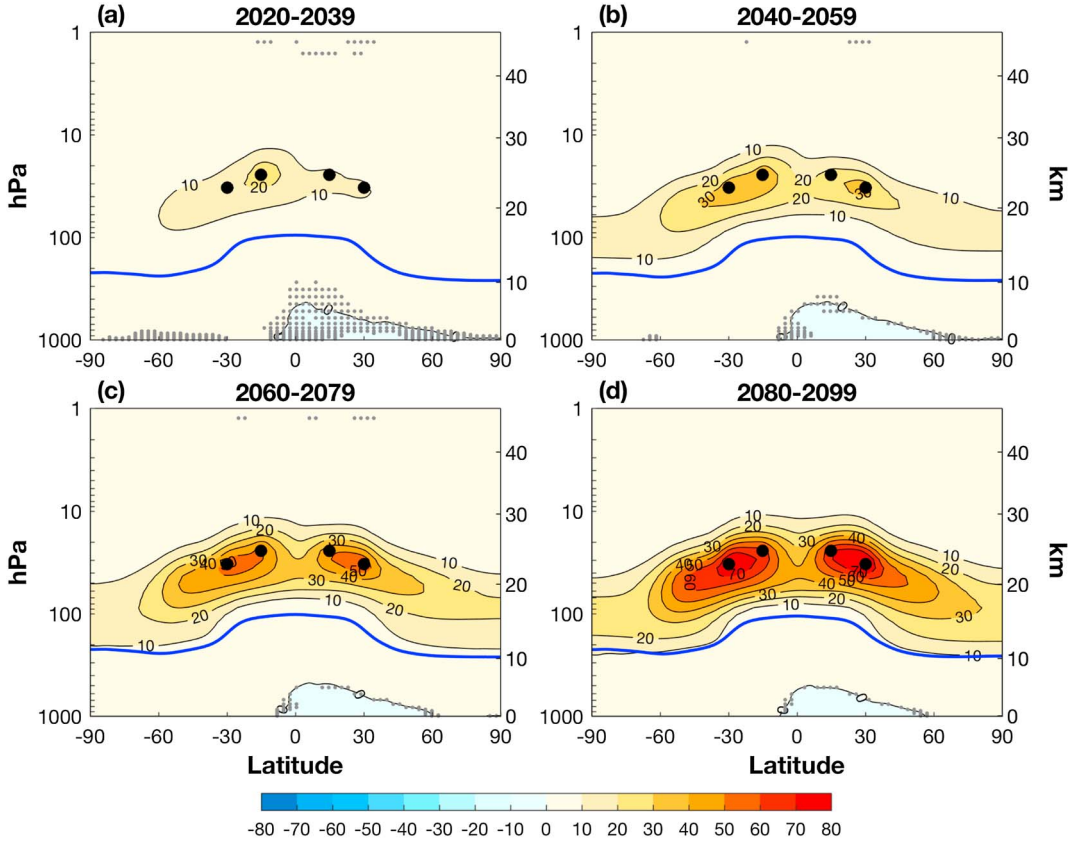

Figure 2. Difference in SO_4 mass mixing ratio between the feedback simulation and the RCP8.5 simulation (2010–2029) averaged over (a) 2020–2039, (b) 2040–2059, (c) 2060–2079, and (d) 2080–2099. Contours are in intervals of 10 μg S/kg air. Black circles depict the locations of SO_2 injections. The blue solid line shows the tropopause in the feedback simulation averaged over the time period denoted above each panel. Areas not statistically significant at the 95% level based on a two-sided Student's *t*-test are stippled.

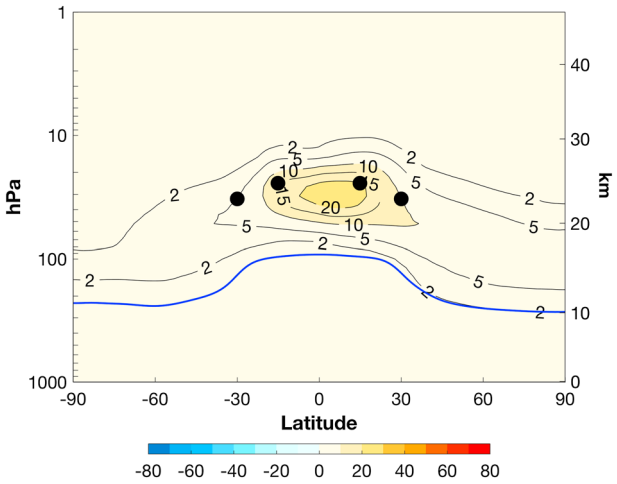

Figure 3. Stratospheric SO_4 mass mixing ratio in the RCP8.5 simulation averaged over year 1992. Contour interval is 2 Tg S/kg air. Contours greater than 10 Tg S/kg air are filled.

the annually averaged SO_4 distribution is quite symmetric between the two hemispheres, with the exception of the Southern Hemisphere (SH) polar regions, which contain less SO_4 than the Northern Hemisphere (NH) polar regions. SO_4 is primarily found equatorward of 60°S, due to a transport barrier near the SH polar jet in austral winter and spring (Niemeier & Schmidt, 2017; Tilmes et al., 2017).

3.2. Mean Dynamical Changes

Stratospheric temperature changes in the feedback simulation relative to RCP8.5 for various time periods are illustrated in Figure S1 in the supporting information and changes relative to the time period 2010–2029 are shown in Figure 4 (All figures in the supporting information show differences between the feedback simulation and RCP8.5 for the same time period). In the RCP8.5 simulation, tropospheric temperatures increase by up to 6 K in the upper tropical troposphere, and the lowermost stratosphere cools by 2 to 4 K (not shown). In the feedback simulation, relative to the RCP8.5 simulation, there is a strong increase in temperature in the tropical lower stratosphere between the injection points and the tropopause (Figure S1). Accompanying changes in ozone are shown in Figure S2. As shown by Richter et al. (2017), stratospheric ozone decreases in the region of highest aerosol concentrations, which reduces the SW heating in that region. Similarly to what was shown in Richter et al. (2017) for single-point injection scenarios, the concentration of ozone decreases near the multiple injections points, decreasing the SW heating in that region (Figure S3) and compensating some of the SW heating increase due to aerosols. On the other hand, the concentration of ozone increases above and below the aerosol layer increasing the shortwave heating rates in those regions (Figure S2).

Due to the processes described above, the stratospheric temperatures are different in the feedback simulation, compared to the reference period of the RCP8.5 simulation (2010 and 2029), especially in the lower stratosphere (Figure 4). The lower stratosphere in the tropics, between 30°S and 30°N between 30 and 100 hPa, is warmer by ~4 K between 2040 and 2059, and by ~8 K by 2080–2099. These changes in the temperature in the lower stratosphere in the feedback simulation grow approximately linearly with the global SO_4 burden and injection amount as shown in Figure 5. Figure 5a shows that the total SO_4 burden in the feedback simulation increases approximately linearly with total SO_2 injection rate. Stratospheric sulfate lifetime (defined as the global stratospheric aerosol burden in Tg S divided by the injection rate in Tg S/year), ranges from ~1.2 years early in the simulation to ~1.0 year toward the end of the century. These values are similar to those found by Tilmes et al. (2017) in simulations with 6 Tg S/year single-point injections, which showed a lifetime of 1.1 (0.94) years for injections at 30°S (30°N) and 1.43 (1.33) years for injections at 15°S (15°N). Figure 5b shows, that despite the complexities of the involved processes, the mean lower tropical stratospheric temperature increases approximately linearly with SO_4 burden, at a rate of 0.38 K/(Tg S) (or 0.19 K per Tg injected SO_2 per year), with a slightly higher warming rate for low SO_4 burden than for high. In addition, the temperature changes seen in this geoengineering simulation with multiple injection locations for a burden of 6 Tg S are similar to those found by Richter et al. (2017) for single-injection locations at 30°S (30°N) and approximate burden of 6 Tg S. This further demonstrates that to a first approximation, the global SO_4 burden determines the degree of lower stratospheric warming as a result of SO_2 injections, despite the complexities of the

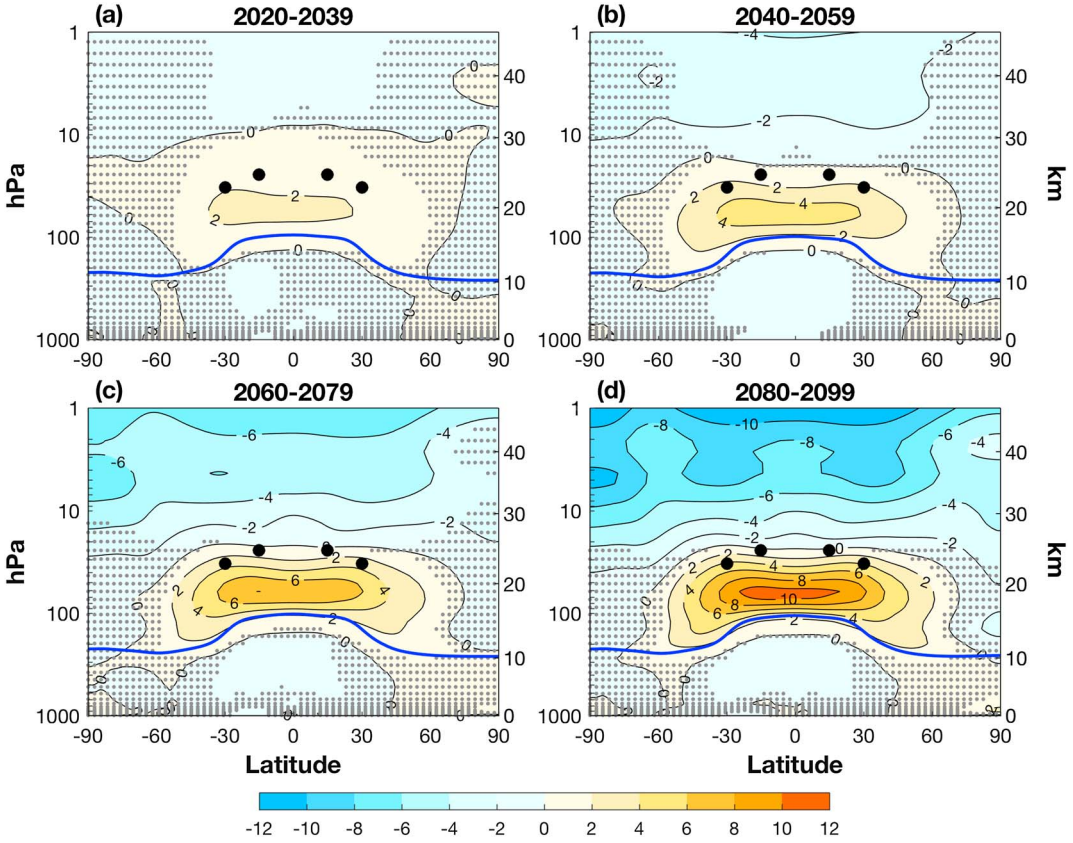

Figure 4. Same as Figure 2 but for zonal and annual mean temperature. Contours are in intervals of 2 K. Areas not statistically significant at the 95% level based on a two-sided Student's *t*-test are stippled.

interactions between the aerosols, chemistry, and dynamics. The upper stratosphere in the feedback simulation is colder as compared to RCP8.5 (2010–2029) at all the latitudes due to the cooling effects of greenhouse gases, which are not offset by geoengineering.

In the feedback simulation, relative to the equivalent time period of RCP8.5, the tropical troposphere cools fairly uniformly with height, with largest cooling in the tropics in the middle to upper troposphere, and slightly more cooling in the NH than in the SH (Figure S1). These changes compensate the warming due to increasing greenhouse gases quite effectively. Figure 4 shows that the temperature throughout the majority of the troposphere in the feedback simulation all the way up to 2099 is not statistically different from the temperature in the RCP8.5 simulation averaged between 2010 and 2029. The exceptions are the tropical middle and upper troposphere, which is colder compared to RCP8.5 (2010–2029), and the polar NH lower troposphere, which is warmer, although the magnitude of these anomalies is still below 2 K.

The large changes in stratospheric temperatures between 30 and 100 hPa, primarily arising from the heating from the aerosol absorption, in the feedback simulation are related to changes in the stratospheric mean zonal wind, as zonal mean wind and temperature must remain in approximate thermal wind balance. Relative to the RCP8.5 simulation, the increased equator-to-pole temperature gradient in the stratosphere causes a strengthening of both the SH and NH polar jets, reaching changes of 8 m/s (SH) and 4 m/s (NH) in an annual mean (Figure S4) and weakening of the subtropical winds near 30°S/30°N between 60 and 130 hPa, as well as weakening of the Tropical winds between 40 and 15 hPa (also discussed in Tilmes et al., 2018).

December, January, February (DJF) zonal mean wind changes are of most relevance to NH storm tracks and stratospheric tropospheric coupling. The DJF zonal mean zonal wind differences in the geoengineering with feedback simulation relative to the RCP8.5 simulation period 2010–2029 are shown in Figure 6. The differences due to geoengineering in DJF zonal mean zonal wind are similar to the differences in the annual mean and other seasons (not shown). Between 2020 and 2039 the differences are mostly small and insignificant in the stratosphere, except for the SH jet (Figure 6a). By the time period 2040 and 2059, significant differences

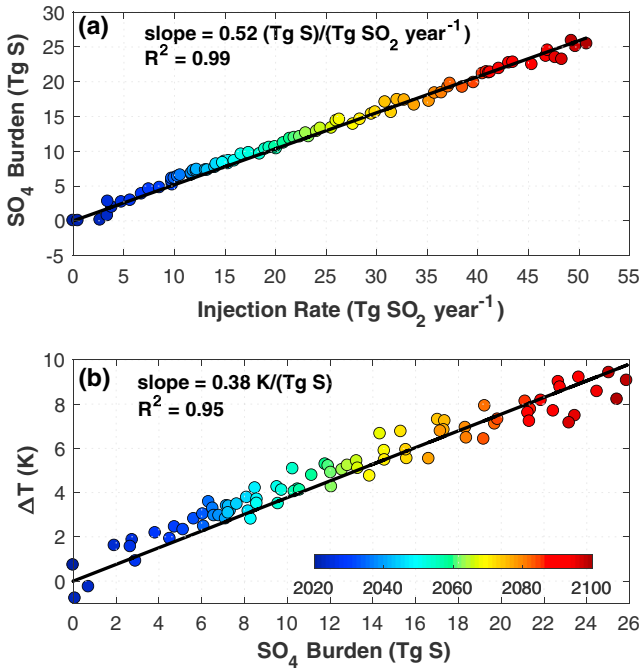

Figure 5. (a) Global SO_4 burden in units of Tg S as a function of SO_2 injection rate for the feedback simulation. (b) Difference in annual and zonal mean temperature averaged over the region between 30°S and 30°N and between 30 and 100 hPa for each year of feedback simulation minus the same for the RCP8.5 (2010–2029 average) versus SO_4 burden. In both panels, each circle represents a single year and the color of the circle indicates the year of injection. Solid black line in each panel depicts the least squares regression line fit through the origin. Slope and R^2 (correlation coefficient squared) are denoted in the top left region of each panel.

between the feedback simulation and RCP8.5 (2010–2029) emerge in the stratosphere: an increase in the strength of the westerly jet in the NH by ~6 m/s and a slow down of the easterly stratospheric winds in the SH by ~4 m/s. In this time period, an easterly wind anomaly appears in the tropics of ~4 m/s, centered at 20 hPa. As more geoengineering is applied, the change in the tropical stratospheric winds grows to 6 m/s by 2080–2099, and the stratospheric extratropical jets speed up, with significant westerly differences of around 8 m/s in both hemispheres. By 2080–2099, the significant easterly anomalies near 100 hPa 30°S and 30°N are also well established. These changes are qualitatively consistent with those found in previous studies such as Tilmes et al. (2009) and Ferraro et al. (2015), but the magnitude of changes is different due to the different simulation/injection setup.

Aside from the above described changes in the stratospheric circulation, small but significant changes also appear in the tropospheric circulation in the feedback simulation relative to the RCP8.5 reference period (Figure 6). A horseshoe-like structure of anomalous easterly winds emerges with anomalies maximizing just above the tropopause in the subtropics, and reaching down into the troposphere. This pattern is similar to the zonal wind anomalies that accompany the easterly phase of the QBO shown by Garfinkel and Hartmann (2011), and it is likely that similar dynamics are at play here. In the feedback simulation, throughout the troposphere, the zonal mean westerlies are reduced at around 45° latitude in both hemispheres, with changes being statistically significant between 2020 and 2039 in the SH, and significant in both hemispheres later in the simulation. Tropospheric winds near 60° are increased. However, they are only statistically significant in the NH between 2080 and 2099 below 600 hPa. These anomalies are in the sense of a weakening and poleward shifting of the midlatitude westerly jet stream in the SH and predominantly a weakening of the jet stream in the NH (compare the wind anomalies with the location of the climatological jet stream, red lines in Figure 6).

Changes in the tropospheric circulation that accompany the warming of the tropical lower stratosphere and the strengthening of the stratospheric westerly jets in the feedback simulation are in agreement with expectations from previous idealized modeling experiments. Haigh et al. (2005) demonstrated that preferential warming of the tropical lower stratosphere results in a poleward shifting of the tropospheric westerlies. Simpson et al. (2009) subsequently proposed a mechanism for this response whereby the propagation of

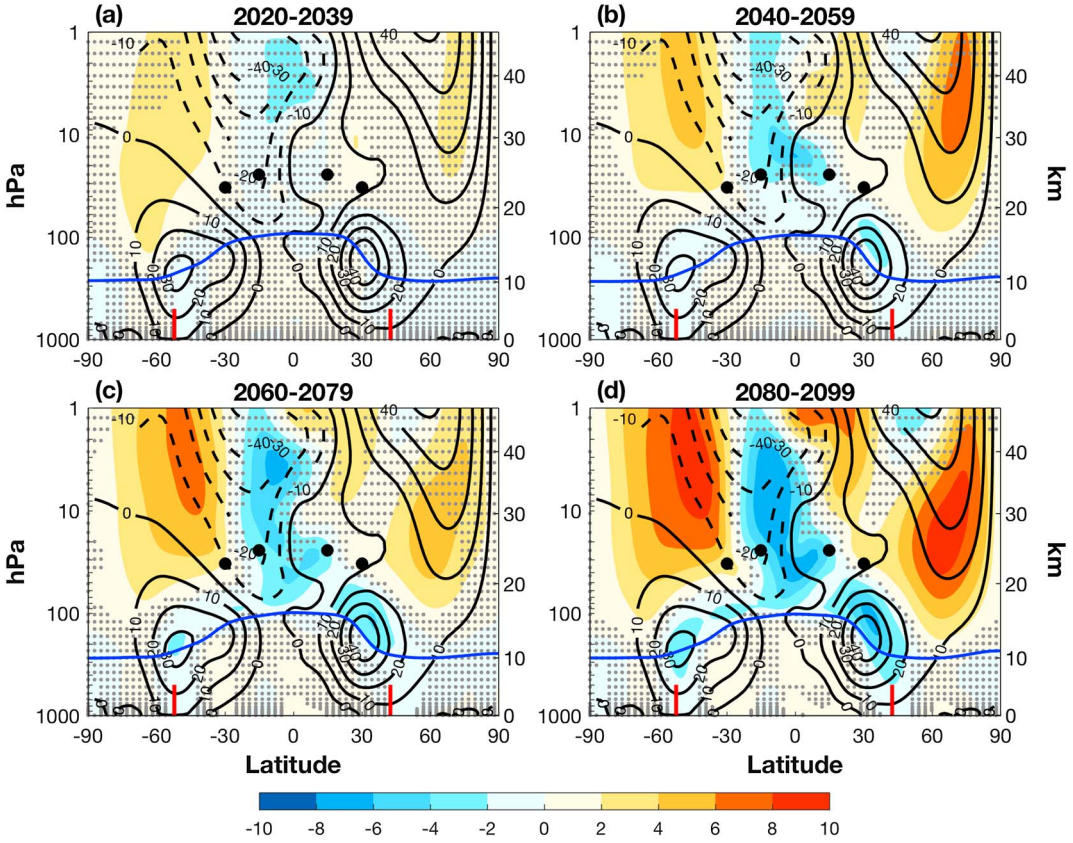

Figure 6. Difference of DJF zonal mean wind in m/s in the feedback simulation relative to the RCP8.5 simulation (2010–2029) averaged over (a) 2020–2039, (b) 2040–2059, (c) 2060–2079, and (d) 2080–2099 (shaded). Contours indicated the DJF zonal mean wind averaged between 2010 and 2029 of the RCP8.5 simulation, with a contour interval of 10 m/s. Black circles depict the locations of SO_2 injections. The red vertical lines indicate the latitude of the tropospheric jet at 850 hPa between 2010 and 2029, calculated as the latitude of the maximum of a quadratic fit to the values at the three grid points centered on the grid point maximum. The blue solid line shows the tropopause in the feedback simulation averaged over the time period denoted above each panel. Areas not statistically significant at the 95% level based on a two-sided Student's *t* test are stippled. DJF = December, January, February.

tropospheric synoptic scale eddies is influenced by altered temperature gradients around the tropopause. It has also been shown that enhanced stratospheric vertical wind shear (Wittman et al., 2007) and strengthening of the stratospheric polar vortex (Polvani & Kushner, 2002) tend to be accompanied by a poleward shifting of the tropospheric westerlies. While the detailed mechanisms at play in these feedback simulations remain to be fully understood, it should be expected, based on the above studies, that the warming of the tropical lower stratosphere, strengthening of the stratospheric vortex and enhanced midlatitude vertical wind shear would conspire to produce the tropospheric zonal wind anomalies shown in Figure 6.

The extent to which the characteristics of tropospheric storm systems in NH winter are altered by the above described wind changes is demonstrated in Figure 7. This figure shows the change in eddy kinetic energy (EKE) along with the local changes in zonal wind on the 700 hPa level. Similarly to Lehmann et al. (2014), EKE is defined here as

$$\mathrm{EKE} = 0.5\,(u'^2 + v'^2) \tag{1}$$

where u' and v' are the daily averaged 2.5–6-day band-pass filtered zonal and meridional wind speeds.

The future changes in zonal wind and EKE found in the RCP8.5 simulation (Figures 7a and 7b) show many of the features common to future projections under this scenario. Namely, there is a strengthening of the westerlies and associated increase in EKE at the exit region of the North Atlantic jet, over western Europe (Chang et al., 2012; Simpson et al., 2014; Woollings & Blackburn, 2012; Zappa et al., 2015) along with a westerly anomaly and enhanced EKE west of the California coast (Chang et al., 2015; Neelin et al., 2013) and a poleward shifting

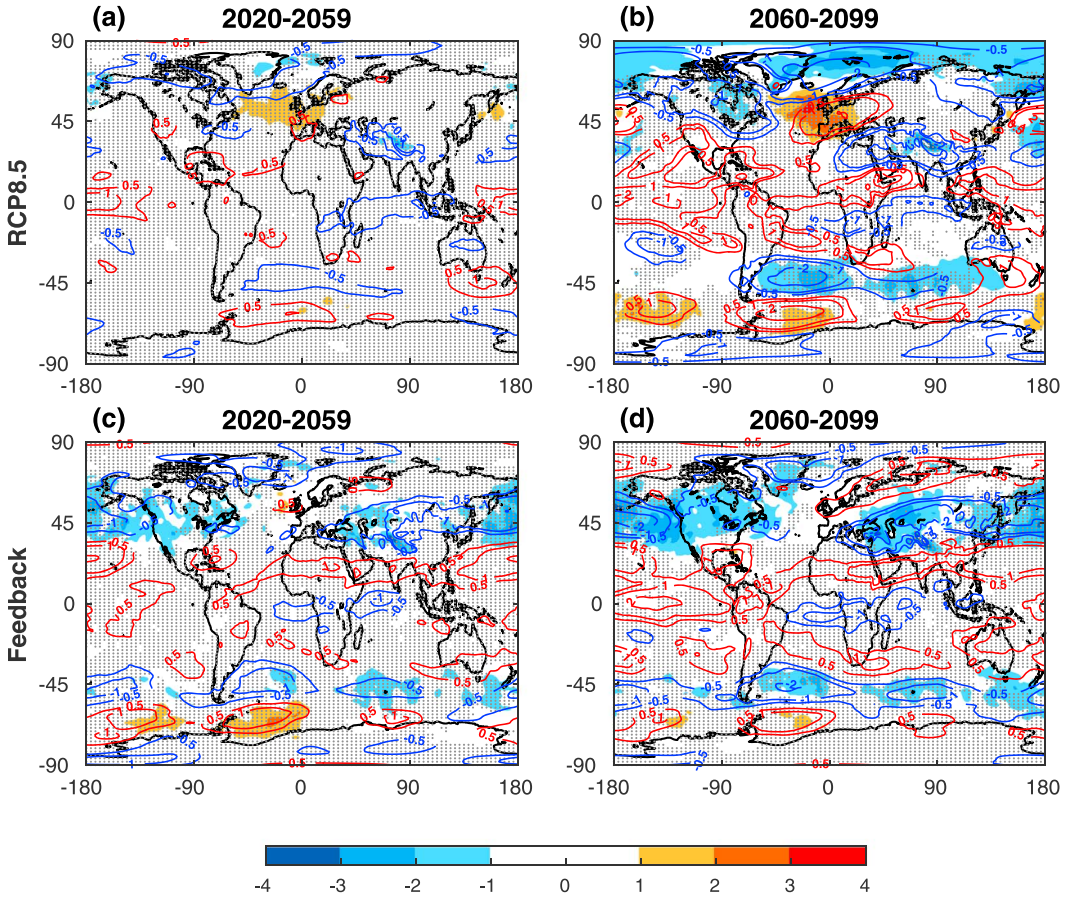

Figure 7. Difference in DJF 700 hPa EKE (colored shading, units of m^2/s^2) and difference in DJF 700 hPa zonal wind (blue and red contours, in intervals of 0.5 of m/s) for (a) RCP8.5 (2020–2059) - RCP8.5 (2010–2029), (b) RCP8.5 (2060–2099) - RCP8.5 (2010–2029), (c) feedback simulation (2020–2059) - RCP8.5 (2010–2029), and (d) feedback simulation (2060–2099) - RCP8.5 (2010–2029) Gray stippling indicate changes not significant at the 95% confidence level based on a two-sided Student's *t* test for EKE. DJF = December, January, February; EKE = eddy kinetic energy.

of the SH storm track (Barnes & Polvani, 2013; Chang et al., 2012). While the changes in EKE are not particularly significant with only one ensemble member presented here, the fact that they have been found in previous model studies and, in the case of the Atlantic extension, that they are present in both time periods shown, lends support to them being a true response to climate change. In the feedback simulation (Figures 7c and 7d), the largest NH changes noted in the RCP8.5 simulation are not present and, instead, there is a general weakening of the storm tracks. This weakening of the EKE corresponds well with regions where the 700 hPa zonal wind decreases relative to RCP8.5 (2010–2029). In the SH, while the weakening of the storm tracks dominates, the poleward shifting of eddy activity accompanying the poleward shifting of the westerlies is more apparent. The mechanisms behind these responses remain to be understood, as do the broader implications for climate on a more regional scale. Ferraro et al. (2015) found in their quadrupled CO_2 simulations with sulfate geoengineering, a poleward shift of the storm tracks in the NH DJF that was much greater than that in their quadrupled CO_2 simulation. Our findings of weakened storm tracks in the NH are different than those of Ferraro et al. (2015). However, Ferraro et al. (2015) found that poleward shifting of the SH jet was amplified in their simulation with quadrupled CO_2 simulation with sulfate geoengineering, similar to our findings for 2020–2059; however, we find that between 2060 and 2099, the poleward shift of the SH storm track in the feedback simulations is the same as that in RCP8.5.

In summary, the geoengineering with feedback simulation meets three surface temperature goals keeping the surface temperature near 2020 levels. However, in order to achieve this with SO_2 injections into the stratosphere, the mean dynamics in the stratosphere change substantially with additional impacts on the tro-

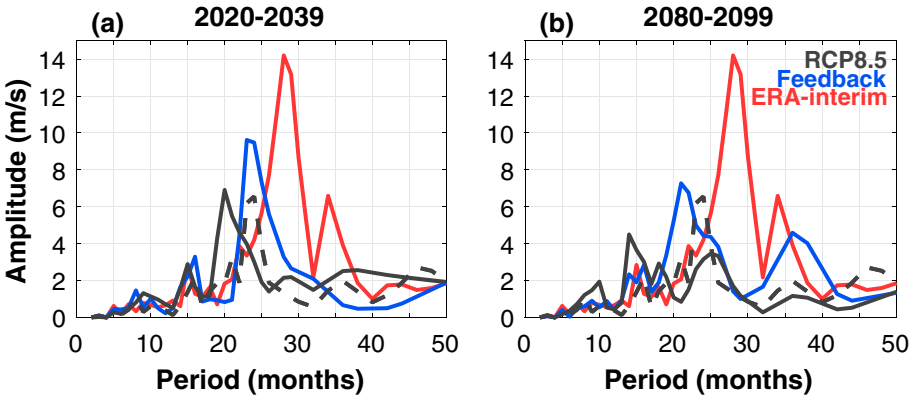

Figure 8. Power spectra of zonal mean zonal wind at 30 hPa for RCP8.5 simulation (thick solid line) and feedback simulation (blue solid line) averaged between 2020 and 2099 (a) and 2080 and 2099 (b). For reference, power spectrum of zonal mean zonal wind at 30 hPa between 1975 and 2015 are shown in both panels for the RCP8.5 simulation (dashed black line) and ERA-Interim analysis (red solid line).

posphere below. In the subsequent sections we examine aspects of stratospheric variability as well as effects on the distribution of water vapor and ozone.

3.3. Stratospheric Variability

Changes in the annual mean zonal mean wind in the tropical stratosphere are associated with changes in the QBO. In our simulations, the period and the amplitude of the QBO are affected by both climate change and geoengineering. Figure 8 shows power spectra of the tropical zonal wind for the RCP8.5 and feedback simulations at 30 hPa. Figure 9 shows the time and height evolution of the tropical zonal mean wind for various time periods as well as ERA-Interim analysis (Dee et al., 2011). Averaged between 1980 and 1999, the QBO has a dominant period of around 24 months, shorter than the observed 28-month period, and it decreases to 20 months when averaged between 2020 and 2039, and to 14 months by the period of 2080–2099 under RCP8.5 scenario. A mean 14-month period of the QBO is smaller than what has ever been seen in the historical record, which started in 1952. In CESM1(WACCM), the properties of convectively generated gravity waves are coupled to the properties of convection. More specifically, the convective heating depth determines the range of phase speeds of gravity waves, and the amplitude of momentum flux is proportional to the square of the amplitude of convective heating (Beres et al., 2004; Richter et al., 2010). These relationships are based on linear theory and verification with simulations of gravity waves by mesoscale (gravity wave resolving) simulations. Hence, in a warming climate, gravity wave momentum flux entering the stratosphere increases due to the increase in the amplitude of tropical convective heating (not shown), and hence acts to shorten the period of the QBO. The shortened period of the QBO in a warming climate is consistent with the study of Giorgetta and Doege (2005). Kawatani et al. (2011) and Watanabe and Kawatani (2012) found the QBO to lengthen in a warming climate, but the parameterized gravity waves in their models do not change with warming climate, as they assume that gravity wave sources are fixed. A study by Schirber et al. (2015) was inconclusive with regard whether the period and amplitude of the QBO will change in warming climate and found that how the QBO was projected to change was dependent on the choice of gravity wave parameterization. The uncertainty in the period of the QBO with warming climate is one of the reasons for the recently launched QBO Initiative (Butchart et al., 2017). While it remains to be confirmed whether the response of the QBO to changing climate in CESM1(WACCM) is realistic, the gravity wave parameterization used was specifically designed to deal with a changing climate.

The QBO in the feedback simulation also changes (Figures 8, 8e, and 9f). However, for the majority of the simulation it remains closer to what is observed in present day than in the RCP8.5 simulation. Between 2020 and 2039, the QBO period is ~23 months, very similar to what it is in the RCP8.5 simulation in present day but shorter than observations, but the amplitude increases by ~25% as illustrated by the power spectra shown in Figure 8a. The change in QBO amplitude primarily comes from the strengthening of the westerly QBO phase (Figure S6c). Between 2080 and 2099, the dominant period of the QBO in the feedback simulation decreases to ~21 months with amplitude similar to that of the RCP8.5 simulation between 1980 and 2000. The 21-month period is shorter than in present day but not nearly as short as in the RCP8.5 simulation during this time.

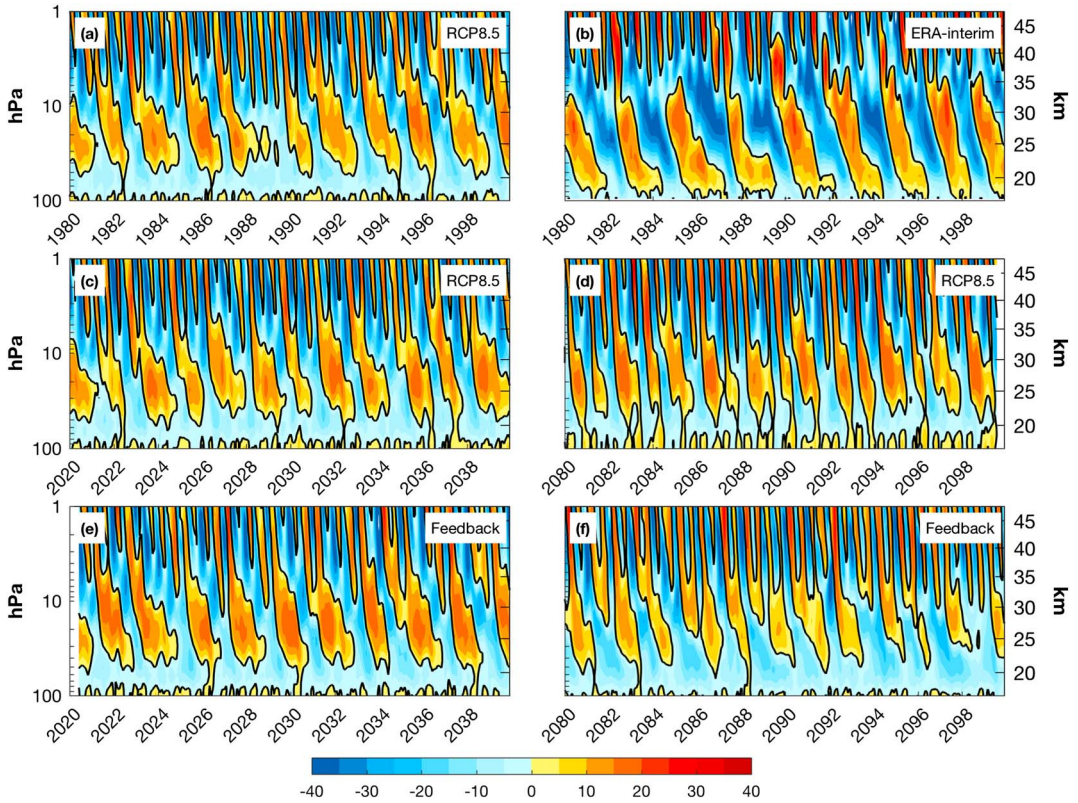

Figure 9. Zonal mean zonal wind averaged between 2°S and 2°N for (a) RCP8.5 simulation between 1980 and 1999, (b) ERA-Interim reanalysis between 1980 and 1999, (c) RCP8.5 simulation between 2020 and 2040, (d) RCP8.5 simulation between 2080 and 2100, (e) feedback simulation between 2020 and 2040, and (f) feedback simulation between 2080 and 2100. Contour interval is 5 m/s.

Richter et al. (2017) showed that SO_2 injections into the stratosphere on one side of the equator (at 15° or 30°) decrease the QBO period to 12 to 17 months. However, when such injections are placed simultaneously on both sides of the equator, the changes to meridional advection nearly balance each other out; hence, the QBO period is less impacted. In our simulation, SO_2 injections are primarily at 30°S and 30°N, hence the residual vertical velocity increases near those location and not in the tropics (not shown); hence, there is no change in the vertical advection term, and hence no impact on the QBO period. Since in the feedback simulations sea surface temperatures and the strength of convection remain at 2020 levels, the gravity wave momentum fluxes also remain at those levels, and the QBO period remains close to 2020 levels.

Although the dominant period of the QBO in the feedback simulation remains close to 2020 levels, the structure of the oscillation changes as illustrated by the comparison of Figure 9f to Figure 9a. As the simulation progresses, easterlies dominate the lower stratosphere and westerly phases become weaker. The increase in tropical easterlies in the lower equatorial stratosphere was also noted in Tilmes et al. (2018) in the case of injections on both sides of the equator and is associated with the change in the zonal mean wind climatology toward a more easterly state, as was shown in Figure 6.

Lastly, changes in the zonal mean wind, particularly in DJF, in the extratropical and polar stratosphere and changes in tropospheric planetary wave activity could affect the frequency of sudden stratospheric warmings (SSWs). A major SSW event is defined as an event where the westerly polar vortex reverses to easterly and the stratospheric polar temperatures rise radically over a period of a few days. SSW events can influence the surface weather for 2 to 8 weeks after an event, inducing a negative North Atlantic Oscillation (NAO) pattern (e.g., Baldwin & Dunkerton, 2001; Polvani et al., 2017). SSWs also lead to poleward ozone transport and slowed ozone depletion in the NH stratosphere. To define SSW events here we use the common definition of Charlton and Polvani (2007), the same as that used in Butler et al. (2017). An SSW event is defined when the zonal mean zonal wind at 60°N, 10 hPa becomes easterly. In order to avoid double counting of events, the 60°N, 10 hPa zonal mean zonal winds must return to westerly for 20 consecutive days between events. Events for which

Table 1
Frequency of Major SSWs in Events per Year (Second Column) for the RCP8.5 and Feedback Simulations Averaged Over 1975–2015 (RCP8.5 only), 2020–2059, and 2060–2099

Simulation and years	SSW Freq	97.5th (%)	2.5th (%)
RCP8.5 1975–2015	0.7	0.9	0.53
RCP8.5 2020–2059	0.44	0.64	0.26
RCP8.5 2060–2099	0.36	0.54	0.20
FDBK 2020–2059	0.49	0.67	0.3
FDBK 2060–2099	0.28	0.46	0.15

Note. The second and third columns show the 97.5th and 2.5th percentiles of sudden stratospheric warming (SSW) frequencies from 1,000 samples of 40 years length derived by using a bootstrapping with replacement methodology from the respective model segment.

the winds do not return to westerly for at least 10 consecutive days before 30 April are not counted as they are considered final warmings.

The SSW frequencies for the RCP8.5 and feedback simulations are shown in Table 1 for various time periods along with results from a bootstrap analysis to estimate the uncertainty in the SSW count for each simulation segment. The 2.5th and 97.5th percentiles of the bootstrap samples for each case are quoted, so a value outside of this range has less than a 5% chance of occurring. Therefore, when the count for a simulation segment lies outside of this range for another, we consider those segments to be significantly different, with the caveat that the uncertain range may be underestimated due to the small number of samples in the analysis. Between 1975 and 2015, the SSW frequency is 0.7 $year^{-1}$, in very good agreement with observed SSW frequency during this time period of 0.6 $year^{-1}$ (e.g., Butler et al., 2017). In both the RCP8.5 and feedback simulations, SSW frequency decreases with time. SSW frequency is 0.44 $year^{-1}$ in RCP8.5 and 0.49 $year^{-1}$ in the feedback simulation between 2020 and 2059, and decreases further to 0.36 $year^{-1}$ in RCP8.5 and 0.28 $year^{-1}$ in the feedback simulation between 2060 and 2099. The results presented here are from only one realization of the RCP8.5 and geoengineering with feedback simulations, and SSW counts can vary between ensemble members of the same model. SSW frequencies in both RCP8.5 and feedback simulations between 2020 and 2059 and 2060 and 2099 are outside of the bootstrapped 2.5th and 97.5th percentiles for RCP8.5 1975–2015, and hence, we consider these to differ significantly from the SSW frequency in the reference period of 1975–2015. It is not clear whether the further decrease of SSW frequency in the feedback simulation between 2060 and 2099 to 0.28 $year^{-1}$ is significant, as this value falls inside of the 2.5th to 97.5th percentile range of RCP8.5 2060–2099, but falls outside of that percentile for the feedback simulation 2020–2059. More ensemble members of these simulations are needed to determine the robustness of these findings; however, the two simulations shown here do not suggest a significant change in the frequency of SSWs in the feedback simulation compared to RCP8.5 for the same time period.

Sudden stratospheric warmings are one measure of changes of the polar vortex, based on a threshold criterion, and the decrease in their frequency does not necessarily mean that the vortex becomes less variable, but it means that the vortex rarely reverses. Figure 10 shows the variability of the polar vortex throughout the year in the RCP8.5 and feedback simulations by showing the daily evolution of 60°N, 10 hPa winds for all the simulation years. Compared to present day (1980 to 2000), the mean winds at 60°N, 10 hPa in the RCP8.5 simulation averaged between 2020 and 2100 change by less than 2 m/s throughout the year. On the other hand, in the feedback simulation, the 60°N, 10 hPa winds are stronger throughout the majority of the year by 2 to 4 m/s, with the exception of the NH spring (April–June). In addition, although variability of the NH vortex winds is in general similar in the feedback simulation compared to the RCP8.5 simulation, the range of extreme values of the polar vortex increases in the feedback simulation. In the feedback simulations, January winds at 60°N, 10 hPa reach values between −10 and −20 m/s in January and early February (not seen in RCP8.5), and reach values in excess of 60 m/s in January and February, also not seen in the RCP8.5 simulation. This suggests that the range of extreme vortex states (positive and negative) is altered in the geoengineering simulation and it should be something that is explored as more similar simulations become available. Ferraro et al. (2015) found little change in variability between their simulations with quadrupled CO_2 and quadrupled CO_2 and sulfate geoengineering; however, their mean winds at 60°N and 10 hPa increased by 40 m/s; hence, the range

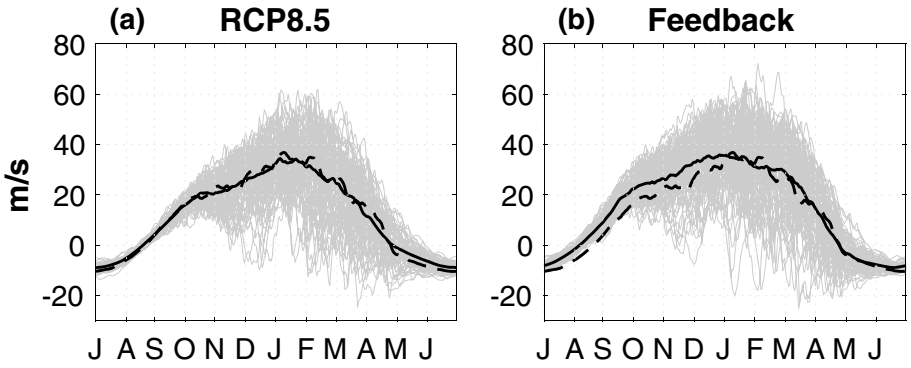

Figure 10. Daily evolution of the zonal mean zonal wind at 60°N, 10 hPa for RCP8.5 (a) and feedback simulation (b). Each gray line shows the wind for each year from 1 July to 30 June. The average of RCP8.5 between 1980 and 2000 is depicted by the dashed line in both panels. The thick solid line shows the average between 2020 and 2100 for RCP8.5 in (a) and feedback in (b).

of vortex states also changed substantially. The above described changes to the polar vortex and SSWs in the geoengineering simulation might affect the NAO. However, given the large internal NAO variability, it is difficult to robustly detect such changes with only one ensemble member of the feedback simulation.

3.4. Water Vapor and Ozone Changes

The warming of the tropical stratosphere and the cooling of the troposphere result in the reduction of the height of the lapse rate tropopause (World Meteorological Organization, 1957) as shown in Figure 11. The tropopause temperature increases in both the RCP8.5 and feedback simulations. The RCP8.5 simulation shows the canonical greenhouse gas response with warming and rising of the tropopause, while the tropopause in the feedback simulation shows an additional temperature increase due to the heating in the aerosol layer. The lapse rate tropopause temperature increase is seasonally uniform in the geoengineering simulation, but not for RCP8.5. In the geoengineering case, the tropopause linearly warms by ~0.83 K per decade, reaching temperatures 5 K warmer in 2080–2099 as compared to 2020–2039. The tropopause in the RCP8.5 case warms by almost 4 K for DJF, while it only warms by 2 K for JJA by the end of the century. This can be described as a weakening of the seasonal cycle and this phenomenon is also seen in other RCP 8.5 simulations (Kim et al., 2013). The seasonal variation of tropopause height changes can be explained by faster upper tropospheric warming concurrent with slower lower stratospheric cooling during DJF as compared to JJA. However, more research is needed to fully understand the processes involved.

Figure 11b shows tropopause pressures/altitudes changes. The tropopause in the RCP8.5 simulation ascends in altitude as the troposphere warms, though the seasonality weakens as discussed earlier. In contrast to this, the tropopause in the feedback simulation descends over 0.5 km by the end of the century, as also shown by

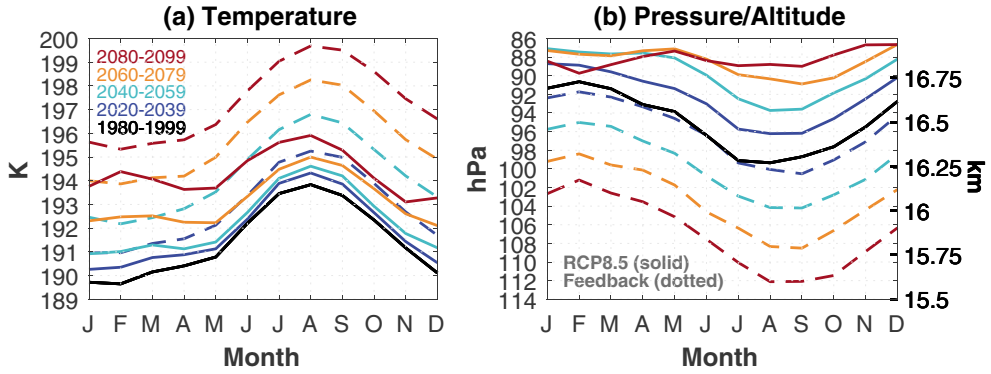

Figure 11. Mean tropical (10°S–10°N) lapse rate tropopause temperature (a) and pressure/altitude (b) for RCP8.5 (solid) and feedback (dashed) simulations for 20-year averages (black (1980–1999), blue (2020–2039), cyan (2040–2059), orange (2060–2079), and red (2080–2099).

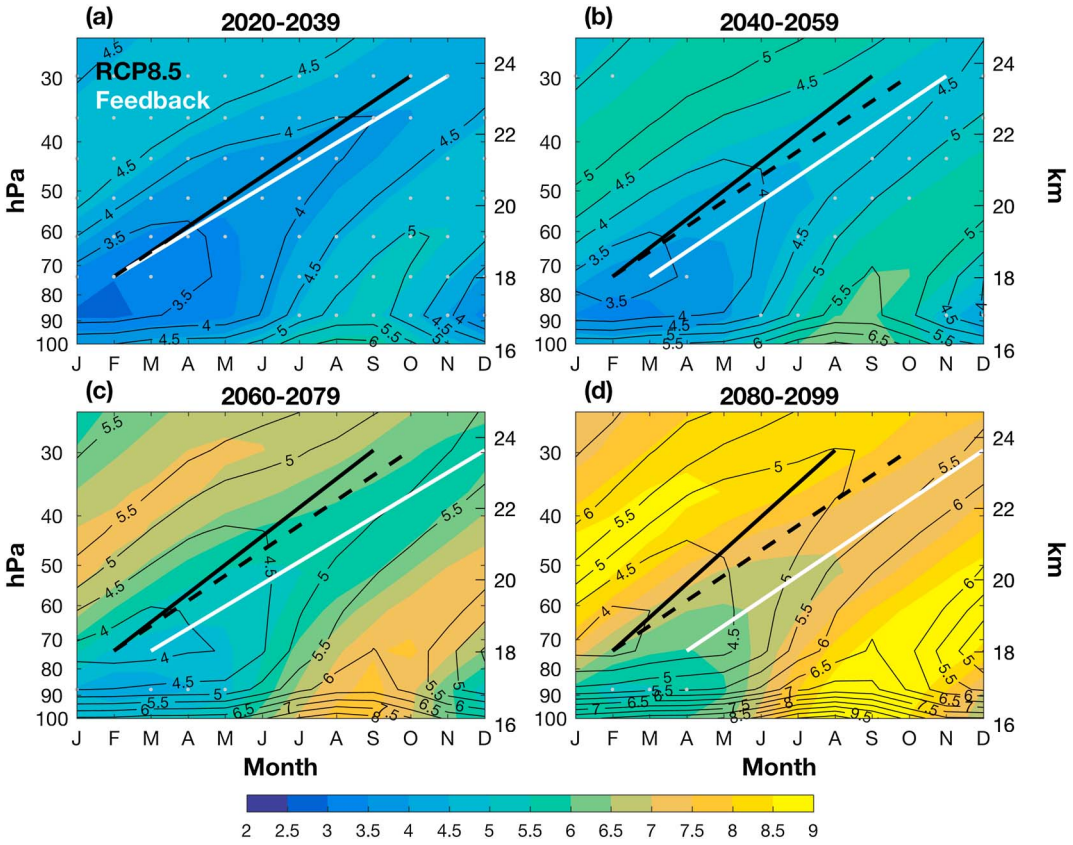

Figure 12. Zonal mean (10°S–10°N) stratospheric water vapor (ppmv) in the feedback simulation (colored contours) superimposed by the RCP8.5 simulation (black contours) averaged over (a) 2020–2039, (b) 2040–2059, (c) 2060–2079, and (d) 2080–2099. Contours are in intervals of 0.5 ppmv. The thick lines follow the minimum water vapor—they therefore broadly showcase the upwelling speed—for the feedback (white) and RCP8.5 (black) simulations. The thick dotted line (same in every panel) represents the upwelling slope in the RCP8.5 simulation averaged over 1980–1999.

Tilmes et al. (2018), likely due to the enhanced aerosol heating just above the present day tropopause, and cooling of the troposphere.

The cold point tropopause changes affect the amount of water vapor entering the stratosphere. Due to a warmer tropopause, the amount of water vapor entering the stratosphere increases in both RCP8.5 and feedback simulations, but much more in the feedback simulation, as shown in Figure 12. In the feedback simulation, in the lower stratosphere annual mean water vapor concentrations are about 4 ppmv between 2020 and 2029 (Figure 12a), whereas by 2080–2099 the annual mean value increases to 5 ppmv in the RCP8.5 simulation (25% increase) and it increases to 7.5 ppmv in the geoengineering simulation (90% increase). Water vapor values near 70 hPa are as high as 9 ppmv in October in the geoengineering simulation between 2080 and 2099. Increases in stratospheric water vapor act to warm the troposphere (Solomon et al., 2010) and the SO_2 injections must also balance the increased longwave radiation—these effects however are difficult to quantify. In addition, ozone destroying odd hydrogen (HO*x* cycle) increases with increasing water vapor, which results in increased ozone depletion, which is most important in spring and summer in the NH lower stratosphere as discussed in Tilmes et al. (2018).

Because water vapor is conserved below the level of methane oxidation (~25 hPa) and above the cold point (~80 hPa), Figure 12 can also be used to analyze tropical upwelling speed via the tape recorder slope (Mote et al., 1998). The thick lines in Figure 12 broadly follow the water vapor minima from 75 hPa to 30 hPa and therefore can be used to approximately quantify the upwelling speed by using the steepness of the slope. The black dashed line in Figure 12 shows the tape recorder slope for present day, which overlaps with that for the RCP8.5 simulation between 2020 and 2039. During the same time period, the feedback simulation shows minor slowing of the tape recorder (white line in Figure 12a). Starting in 2040, the slope of the tape recorder in the feedback simulation (white line) begins to shift later into the seasonal cycle. While it seems this would

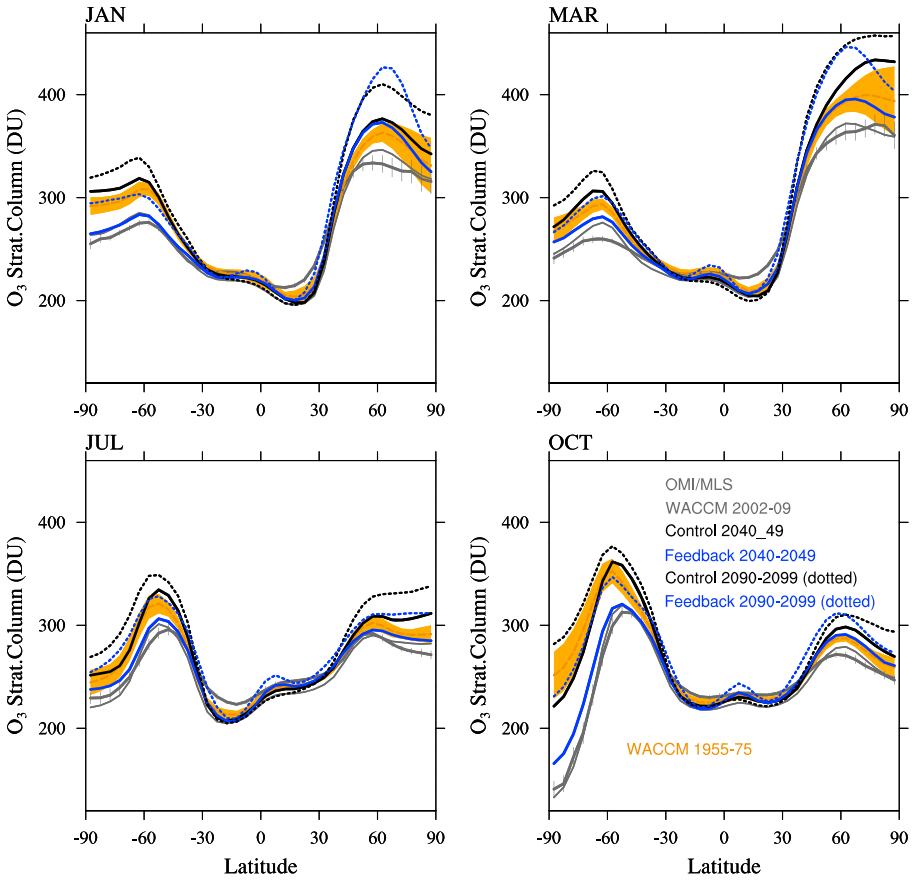

Figure 13. Monthly and zonally averaged stratospheric ozone column (in DU) comparison between OMI/MLS observations between 2004 and 2010 (gray), and CESM1(WACCM) simulations (for ozone > 150 ppb in the model): RCP8.5 between 2004 and 2010 (gray dashed lines), RCP8.5 (black), and feedback simulation (blue) between 2040 and 2049 (thick lines) and between 2090 and 2099 (dotted lines), for January, March, July, and October (different panels). Error bars for the observations in gray describe the zonally averaged 2 sigma 6-year root-mean-square standard error of the mean at a given grid point, derived from the gridded product (Ziemke et al., 2011). Model results are interpolated to the same grid, and error bars (only shown for the control simulations) indicate the standard deviation of the interannual variability per latitude interval. CESM1(WACCM) results between 1955 and 1975 that indicate preozone hole conditions are shown in orange including standard deviation (shading).

indicate further slowing of the tape recorder, that is not the case as the slope actually equals that of present day, and residual vertical velocity in the tropics in the stratosphere during this time period (not shown) is almost the same as that between 2010 and 2030. Because the tropopause is lower in the feedback simulation, the base of the tape recorder is also lower, and therefore, the minimum in water vapor appears later in the seasonal cycle. Using a tropopause-relative framework confirms our results: the upwelling in the feedback simulation below the injection location of 30 hPa remains near that of present day, while the upwelling in RCP8.5 is ~30% faster by 2100, in agreement with past studies (Butchart, 2014).

The injections of SO_2 into the stratosphere also affect ozone, as was shown in Figure S2. Ozone changes as a result of SO_2 injections are the result of both changes in chemistry and dynamics, as described in more detail by Tilmes et al. (2018) for continuous injections at 15°N and 15°S between 2040 and 2049. Column ozone is expected to increase, in particular, in high latitudes following the RCP8.5 scenario (Butler et al., 2016) and reach well above preozone hole conditions in middle to high latitudes by the end of the century (Figure 13, black dotted lines compared to orange area). The decline of ozone depleting substances (ODS) by the end of the century is expected to result in less ozone loss in high polar latitudes and a recovery of the ozone hole by midcentury. However, in the feedback simulation, the continuously growing stratospheric aerosol burden and accompanying surface area density changes result in column ozone values close to what is observed for present day (Figure 13, blue thick lines compared to gray lines). By the end of the century, column ozone values in the feedback simulation are closer to preozone hole conditions for SH middle and high latitudes as

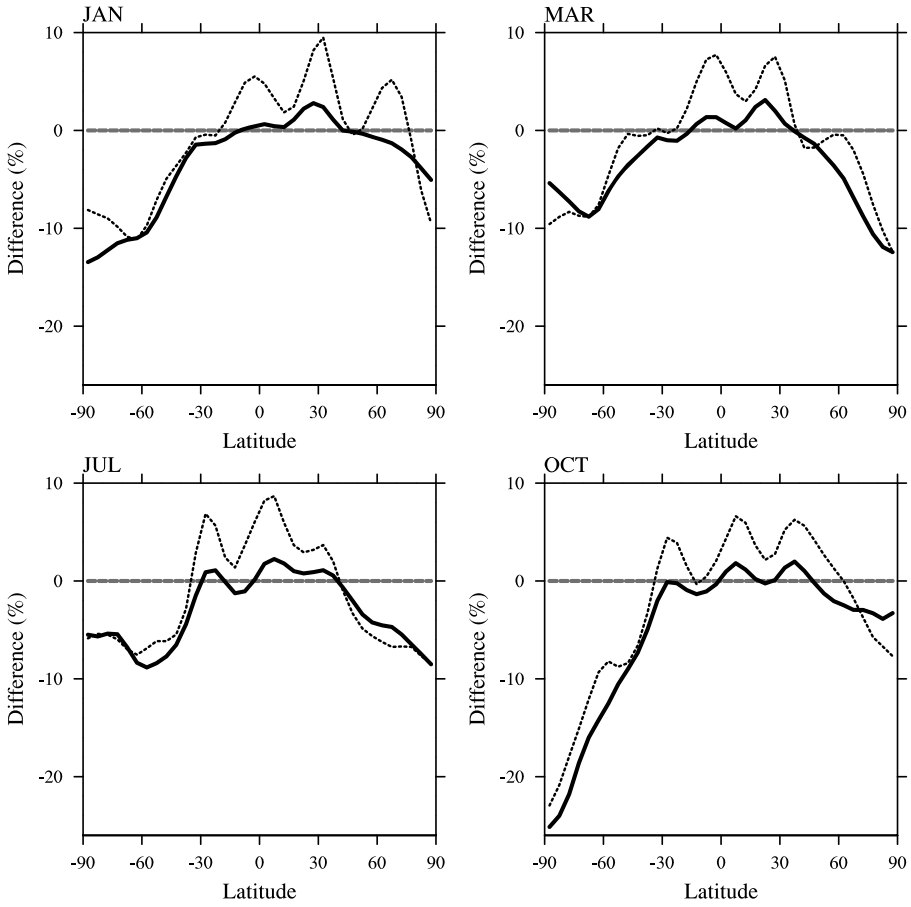

Figure 14. Differences in monthly and zonally averaged stratospheric ozone column (in DU) between feedback and RCP8.5 simulations for different months (different panels) as shown in Figure 13, in 2040–2049 (thick lines) and 2090–2099 (dotted lines).

compared to the RCP8.5 simulation. In contrast to the RCP8.5 simulation, where column ozone levels reach above preozone hole condition, in the feedback simulation, large injection of SO_2 and the strong increase in aerosol burden lead to increased chemical ozone depletion. For the NH middle and high latitudes, strongly increased aerosol burden does not lead to strong reductions in column ozone despite increased chemical ozone depletion, but in part lead to an increase in column ozone in the feedback simulation compared to RCP8.5 as discussed in Tilmes et al. (2018). Differences in column ozone between RCP8.5 and the feedback simulation for the two time periods 2040–2049 and 2090–2099 are rather similar, especially for high latitudes, despite large differences in ODS for both these periods (Figure 14). The increasing aerosol burden in the feedback simulation results in increased chlorine activation through heterogeneous reactions and is likely counteracting the reduced amount of available halogen burden in the stratosphere, however more research is needed to confirm the contributions of these factors versus the role of dynamical feedbacks. The reduction in column ozone in the feedback simulation relative to RCP8.5 in the SH reaches up to 25% in October and between 7% and 12% for the other seasons (for both 2040–2049 and 2090–2099). In the NH, the decrease in ozone reaches up to 12% in March and around 5%–10% for the other seasons. On the other hand, ozone in the tropics in the feedback simulation is increased by the end of the century by 4%–8% compared to RCP8.5, whereas it is similar between 2040 and 2049.

4. Summary and Conclusions

We examined here changes to the dynamics and chemistry of the stratosphere in a first century-long geoengineering simulation in which SO_2 injections were chosen to keep the mean surface temperature near 2020 levels against an RCP8.5 emission scenario. SO_2 injections were placed at 30°S/30°N at ~23 km and 15°S/15°N at ~25 km, and the amount of injection at each location was varied annually using a feedback

algorithm to keep the global annual mean, the equator-to-pole and interhemispheric surface temperature gradients nearly constant. The geoengineering strategy employed here is different from previous sulfate aerosols geoengineering studies in two main aspects: first, in previous studies aerosols were prescribed with fixed distributions or injected at or in regions near the equator. Here the injections are primarily at 30°S and 30°N. Second, in previous studies the location of injection or prescribed aerosols was fixed, and the injection rate was the same or followed a prescribed time dependence, whereas. in our simulation the magnitude of SO_2 injections is adjusted every year to keep the zonal mean surface temperatures near 2020 levels. We find that although the three surface temperature goals were met in our simulation, the approach still significantly alters the mean stratospheric dynamics and variability. Changes in the mean dynamics and chemistry of the stratosphere in our study are qualitatively similar to those found in Tilmes et al. (2018) for constant multiple injections at 15°S and 15°N, and previous studies such as Ferraro et al. (2015); however, we show that details of how geoengineering is done, primarily the location and amount of SO_2 injections, matter for changes in stratospheric and tropospheric variability, as our findings in several aspects of the simulation differ from what has been previously found, including changes in stratospheric winds, QBO, and storm tracks. The feedback mechanism controlling amount of SO_2 injection at four locations is a novel aspect of the geoengineering simulation presented here, and its purpose is to keep the global mean surface temperature, the equator-to-pole and interhemispheric temperature gradients at 2020 levels. In the simulation presented here, the feedback algorithm primarily chooses injections at 30°S and 30°N throughout the simulation, hence the impacts we find here in the stratosphere and upper troposphere are qualitatively the same as would be in a simulation with constant injections at those latitudes. However, the inclusion of the feedback algorithm allows for learning what the right injections rates are to keep surface temperature near 2020 levels, and quantification of stratospheric and tropospheric changes under various injection scenarios.

Changes to the stratosphere in our simulation are most apparent when the total SO_2 injection amount is increased over 20 Tg SO_2/year. The injection of ~20 Tg SO_2/year spread among the four injection sites causes an increase of mean lower stratospheric tropical temperatures of ~4 K, whereas a mean injection of 40 Tg SO_2/year induces an increase of ~8 K in lower stratospheric tropical temperature. The largest increases in stratospheric temperatures occur between 30°S and 30°N, similarly to previous studies which injected SO_2 or prescribed aerosols at or near the equator. We find that the lower stratospheric temperatures in the geoengineering simulation increase approximately linearly with the total SO_4 burden. Changes in tropical lower stratospheric temperature influence the stratospheric circulation and the zonal mean wind. In the geoengineering with feedback simulation, relative to 2010–2029, there is an increase in the strength of the SH and NH stratospheric polar jets reaching 6 m/s in NH and 4 m/s in the SH with ~20 Tg/year total SO_2 injection (period 2040–2059). These changes increase to 8 m/s in both hemispheres with an ~40 Tg/year total SO_2 injection (period 2080–2099). These changes are smaller than those reported by Ferraro et al. (2015) in their quadrupled CO_2 and sulfate simulation with aerosols primarily distributed near the equator, who reported changes in stratospheric NH jets up to 36 m/s. In addition to changes in the polar jets, a decrease in the strength of the subtropical jets begins to occur in the NH lower stratosphere between 2040 and 2059, and a decrease in mean tropical winds by 4 m/s appear in the lower stratosphere affecting the QBO (discussed below). The subtropical lower stratospheric zonal mean winds weaken further in the NH and SH as SO_2 injection amount is increased. In the troposphere, the zonal mean wind weakens on the equatorward side of the midlatitude westerlies and strengthens poleward of 60° latitude in the feedback simulation. This change was found to be accompanied by a predominant weakening of the storm tracks in the NH and a weakening and poleward shifting of storm track activity in the SH compared to 2010–2030, demonstrating that keeping surface temperature near 2020 levels does not necessarily mean that other aspects of tropospheric climate will remain at 2020 levels. Our findings of weakened storm tracks in the NH are different than those found by Ferraro et al. (2015). In the first half of our simulation changes in SH storm tracks are consistent with Ferraro et al. (2015); however, it is not in the second part.

Variability of the polar winter vortex in the NH relative to 1975–2015 is changed in the feedback and RCP8.5 simulations as reflected by a significant decrease in the frequency of SSWs in 2020–2059 and 2060–2099. However, SSW counts in the feedback and RCP8.5 simulations are not statistically different from each other. We found that the range of extreme states of the vortex (strong and weak) in the feedback simulation has increased compared to the RCP8.5 simulation. However, more ensembles are needed to assess robustness of these changes and impacts of these changes on tropospheric weather extremes related to SSW events and the NAO.

Previous studies have shown that the primary mode of stratospheric tropical variability, the QBO, may substantially lengthen or even disappear as a result of SO_2 injections into the stratosphere (Aquila et al., 2014; Niemeier & Schmidt, 2017). In those studies SO_2 injections were placed in the tropics and caused substantial changes to the tropical residual vertical velocity, and hence vertical advection of the mean zonal flow, which were responsible for the changes to the QBO. In our simulation the QBO period becomes progressively shorter in the RCP8.5 simulation; however, throughout the entire geoengineering simulation with SO_2 injections controlled by the feedback algorithm, the QBO period remains close to the present day QBO period. This is because in our simulation the feedback algorithm selected SO_2 injections primarily at 30°S and 30°N, and residual vertical velocity increased near the injection sites, but not right at the equator, similarly as was shown in Richter et al. (2017) for a simulation with constant injections at multiple locations. However, as SO_2 injection amount increases in the feedback simulation, easterlies become stronger in the lower stratosphere and the westerly QBO phase weakens.

We find that the tropopause is affected in both RCP8.5 and geoengineering with feedback simulations. The annual mean temperature increases by ~5 K in the geoengineering simulation and by ~3 K in the RCP8.5 simulation. Nonetheless, geoengineering helps to retain the amplitude of the seasonal cycle of the tropopause, whereas the annual cycle nearly disappears in the RCP8.5 simulation by the end of the century. Following the tropopause temperature changes, annual stratospheric water vapor increases by about 25% in the RCP8.5 simulation, while it increases by 90% in the geoengineering simulation by the end of the century. By the end of the century, geoengineering successfully keeps tropical upwelling speed below 30 hPa near that of present day while it increases by about 30% in the RCP8.5 simulation.

Stratospheric ozone has been impacted in the geoengineering simulation by changes in the stratospheric aerosol burden. Decreased Antarctic column ozone of 20%–24% has been reached in October compared to RCP8.5 for both middle and late 21st century and up to 12% over the Arctic in March. Column ozone has recovered to preozone hole conditions in the feedback simulation, despite the very large injection amounts. In northern middle and high latitudes, column ozone reaches above preozone hole levels, and in winter it reaches even above values derived for RCP8.5. In summary, column ozone changes in our feedback simulation are qualitatively aligned with findings from earlier results (e.g., Pitari et al., 2014; Tilmes et al., 2009, 2018), showing a delay in the recovery in high latitudes; however, magnitudes of changes are different due to different SO_2 injection scenarios. In contrast to Tilmes et al. (2018), where larger injections were used in 2040–2049, this study shows somewhat smaller reduction in column ozone in winter and spring high latitudes, and a smaller response to dynamical changes of column ozone in winter northern latitudes, due to the much smaller heating in the lower tropical stratosphere.

The changes in stratospheric and tropospheric climate presented here are potential side effects of geoengineering using stratospheric aerosols with the goal of keeping multiple surface temperature goals near constant. These conclusions are for an increasing amount of geoengineering to balance the effects of RCP8.5. Ideally, such a geoengineering strategy would be applied in a scenario that would also include strong mitigation efforts of greenhouse gases, and hence, the amount of geoengineering needed would be capped at one of the smaller values described here. The results presented here in many ways show the range of possible side effects of keeping surface temperatures near 2020 levels with stratospheric sulfate geoengineering, and the extent in which side effects of geoengineering change with increased greenhouse emissions and increased SO_2 injections. More realistic scenarios under which geoengineering might be applied that include strong mitigation efforts will be considered in the future. Lastly, although we use a state-of-the art model whose atmospheric, aerosol, and chemistry modules have been extensively verified, there is a need to verify the presented findings with different modeling frameworks to reduce uncertainty.

Acknowledgments
All simulations were carried out on the Yellowstone high-performance computing platform (Computational and Information Systems Laboratory, 2012) and are available to the community via the Earth System Grid at https://doi.org/10.5065/D6X63KMM. The National Center for Atmospheric Research is sponsored by the National Science Foundation. The Pacific Northwest National Laboratory is operated for the U.S. Department of Energy by Battelle Memorial Institute under contract DE-AC05-76RL01830. This research was developed with funding from the Defense Advanced Research Projects Agency (DARPA). The views, opinions, and/or findings expressed are those of the authors and should not be interpreted as representing the official views or policies of the Department of Defense or the U.S. Government.

References

Aquila, V., Garfinkel, C. I., Newman, P. A., Oman, L. D., & Waugh, D. W. (2014). Modifications of the quasi-biennial oscillation by a geoengineering perturbation of the stratospheric aerosol layer. *Geophysical Research Letters*, *41*, 1738–1744. https://doi.org/10.1002/2014GL059919

Baldwin, M. P., & Dunkerton, T. J. (2001). Stratospheric harbingers of anomalous weather regimes. *Science*, *294*, 581–584.

Ban-Weiss, G. A., & Caldeira, K. (2010). Geoengineering as an optimization problem. *Environmental Research Letters*, *5*(3), 34009. https://doi.org/10.1088/1748-9326/5/3/034009

Barnes, E. A., & Polvani, L. (2013). Response of the midlatitude jets, and of their variability, to increased greenhouse gases in the CMIP5 models. *Journal of Climate*, *26*(18), 7117–7135. https://doi.org/10.1175/JCLI-D-12-00536.1

Beres, J. H., Alexander, M. J., & Holton, J. R. (2004). A method of specifying the gravity wave spectrum above convection based on latent heating properties and background wind. *Journal of the Atmospheric Sciences*, *61*, 324–337.

Beres, J. H., Garcia, R. R., Boville, B. A., & Sassi, F. (2005). Implementation of a gravity wave source spectrum parameterization dependent on the properties of convection in the Whole Atmosphere Community Climate Model (WACCM). *Journal of Geophysical Research*, *110*, D10108. https://doi.org/10.1029/2004JD005504

Butchart, N. (2014). The Brewer-Dobson circulation. *Review of Geophysics*, *52*, 157–184. https://doi.org/10.1002/2013RG000448

Butchart, N., Anstey, J. A., Hamilton, K., Osprey, S., Mclandress, C., Bushell, C., et al. (2017). Overview of experiment design and comparison of models participating in phase 1 of the SPARC quasi-biennial oscillation initiative (QBOi). *Geoscientific Model Development*, *11*, 1009–1032. https://doi.org/10.5194/gmd-2017-187

Butler, A. H., Arribas, A., Athanassiadou, M., Baehr, J., Calvo, N., Charlton-Perez, A., et al. (2016). The climate-system historical forecast project: Do stratosphere-resolving models make better seasonal climate predictions in boreal winter?. *Quarterly Journal of the Royal Meteorological Society*, *142*, 1413–1427. https://doi.org/10.1002/qj.2743

Butler, A. H., Sjoberg, J. P., Seidel, D. J., & Rosenlof, K. H. (2017). A sudden stratospheric warming compendium. *Earth System Science Data*, *9*(1), 63–76. https://doi.org/10.5194/essd-9-63-2017

Chang, E. K. M., Guo, Y., & Xia, X. (2012). CMIP5 multimodel ensemble projection of storm track change under global warming. *Journal of Geophysical Research*, *117*, D23118. https://doi.org/10.1029/2012JD018578

Chang, E. K., Zheng, C., Lanigan, P., Yau, A. M., & Neelin, J. D. (2015). Significant modulation of variability and projected change in California winter precipitation by extratropical cyclone activity. *Geophysical Research Letters*, *42*, 5983–5991. https://doi.org/10.1002/2015GL064424

Charlton, A. J., & Polvani, L. M. (2007). A new look at stratospheric sudden warmings. Part I: Climatology and modeling benchmarks. *Journal of Climate*, *20*, 449–469.

Computational and Information Systems Laboratory (2012). Yellowstone: IBM iDataPlex system (NCAR strategic capability projects). http://n2t.net/ark:/85065/d7wd3xhc

Crutzen, P. J. (2006). Albedo enhancement by stratospheric sulfur injections: A contribution to resolve a policy dilemma?. *Climatic Change*, *77*(3-4), 211–219. https://doi.org/10.1007/s10584-006-9101-y

Curry, C. L., Sillmann, J., Bronaugh, D., Alterskjaer, K., Cole, J. N., Ji, D., et al. (2014). A multimodel examination of climate extremes in an idealized geoengineering experiment. *Journal of Geophysical Research: Biogeosciences*, *119*, 3900–3923. https://doi.org/10.1002/2013JD020648

Dee, D., Uppala, S. M., Simmons, A. J., Berrisford, P., Poli, P., Kobayashi, S., et al. (2011). The ERA-Interim reanalysis: Configuration and performance of the data assimilation system. *Quarterly Journal of the Royal Meteorological Society*, *137*, 553–597. https://doi.org/10.1002/qj.828

Driscoll, S., Bozzo, A., Gray, L. J., Robock, A., & Stenchikov, G. (2012). Coupled Model Intercomparison Project 5 (CMIP5) simulations of climate following volcanic eruptions. *Journal of Geophysical Research*, *117*, D17105. https://doi.org/10.1029/2012JD017607

English, J. M., Toon, O. B., & Mills, M. J. (2012). Microphysical simulations of sulfur burdens from stratospheric sulfur geoengineering. *Atmospheric Chemistry and Physics*, *12*(10), 4775–4793. https://doi.org/10.5194/acp-12-4775-2012

Ferraro, A. J., Charlton-Perez, A. J., & Highwood, E. J. (2015). Stratospheric dynamics and midlatitude jets under geoengineering with space mirrors and sulfate and titania aerosols. *Journal of Geophysical Research: Atmospheres*, *120*, 414–429. https://doi.org/10.1002/2014JD022734

Ferraro, A. J., Highwood, E. J., & Charlton-Perez, A. J. (2011). Stratospheric heating by potential geoengineering aerosols. *Geophysical Research Letters*, *38*, L24706. https://doi.org/10.1029/2011GL049761

Garfinkel, C. I., & Hartmann, D. L. (2011). The influence of the quasi-biennial oscillation on the troposphere in winter in a hierarchy of models. Part II: Perpetual winter WACCM runs. *Journal of the Atmospheric Sciences*, *68*(9), 2026–2041. https://doi.org/10.1175/2011JAS3702.1

Giorgetta, M. A., & Doege, M. C. (2005). Sensitivity of the quasi-biennial oscillation to CO_2 doubling. *Geophysical Research Letters*, *32*, L08701. https://doi.org/10.1029/2004GL021971

Haigh, J. D., Blackburn, M., & Day, R. (2005). The response of tropospheric circulation to perturbations in lower-stratospheric temperature. *Journal of Climate*, *18*(17), 3672–3685. https://doi.org/10.1175/JCLI3472.1

Heckendorn, P., Weisenstein, D., Fueglistaler, S., Luo, B. P., Rozanov, E., Schraner, M., et al. (2009). The impact of geoengineering aerosols on stratospheric temperature and ozone. *Environmental Research Letters*, *4*(4), 45108. https://doi.org/10.1088/1748-9326/4/4/045108

Jones, A. C., Haywood, J. M., & Jones, A. (2016). Climatic impacts of stratospheric geoengineering with sulfate, black carbon and titania injection. *Atmospheric Chemistry and Physics*, *16*(5), 2843–2862. https://doi.org/10.5194/acp-16-2843-2016

Kawatani, Y., Hamilton, K., & Watanabe, S. (2011). The quasi-biennial oscillation in a double CO_2 climate. *Journal of the Atmospheric Sciences*, *68*(2), 265–283. https://doi.org/10.1175/2010JAS3623.1

Kim, J., Grise, K. M., & Son, S. W. (2013). Thermal characteristics of the cold-point tropopause region in CMIP5 models. *Journal of Geophysical Research: Atmospheres*, *118*, 8827–8841. https://doi.org/10.1002/jgrd.50649

Kinnison, D. E., Brasseur, G. P., Walters, S., Garcia, R. R., Marsh, D. R., Sassi, F., et al. (2007). Sensitivity of chemical tracers to meteorological parameters in the MOZART-3 chemical transport model. *Journal of Geophysical Research*, *112*, D20302. https://doi.org/10.1029/2006JD007879

Kravitz, B., Caldeira, K., Boucher, O., Robock, A., Rasch, P. J., Alterskjær, K., et al. (2013). Climate model response from the Geoengineering Model Intercomparison Project (GeoMIP). *Journal of Geophysical Research: Atmospheres*, *118*, 8320–8332. https://doi.org/10.1002/jgrd.50646

Kravitz, B., MacMartin, D. G., Mills, M. J., Richter, J. H., Tilmes, S., Lamarque, J.-F., et al. (2017). First simulations of designing stratospheric sulfate aerosol geoengineering to meet multiple simultaneous climate objectives. *Journal of Geophysical Research: Atmospheres*, *122*, 12,616–12,634. https://doi.org/10.1002/2017JD026874

Kravitz, B., Macmartin, D. G., Wang, H., & Rasch, P. J. (2016). Geoengineering as a design problem. *Earth System Dynamics*, *7*(2), 469–497. https://doi.org/10.5194/esd-7-469-2016

Kravitz, B., Robock, A., Boucher, O., Schmidt, H., Taylor, K. E., Stenchikov, G., & Schulz, M. (2011). The Geoengineering Model Intercomparison Project (GeoMIP). *Atmospheric Science Letters*, *12*(2), 162–167. https://doi.org/10.1002/asl.316

Lehmann, J., Coumou, D., Frieler, K., Eliseev, A. V., & Levermann, A. (2014). Future changes in extratropical storm tracks and baroclinicity under climate change. *Environmental Research Letters*, *9*, 84002. https://doi.org/10.1088/1748-9326/9/8/084002

Liu, X., Easter, R. C., Ghan, S. J., Zaveri, R. A., & Rasch, P. J. (2012). Toward a minimal representation of aerosols in climate models: Description and evaluation in the Community Atmosphere Model CAM5. *Geoscientific Model Development*, *5*(3), 709–739.

MacMartin, D. G., Keith, D. W., Kravitz, B., & Caldeira, K. (2013). Management of trade-offs in geoengineering through optimal choice of non-uniform radiative forcing. *Nature Climate Change*, *3*(4), 365–368. https://doi.org/10.1038/nclimate1722

MacMartin, D. G., Kravitz, B., Keith, D. W., & Jarvis, A. (2014). Dynamics of the coupled human-climate system resulting from closed-loop control of solar geoengineering. *Climate Dynamics*, *43*, 243–258. https://doi.org/10.1007/s00382-013-1822-9

MacMartin, D. G., Kravitz, B., Tilmes, S., Richter, J. H., Mills, M. J., Lamarque, J.-F., et al. (2017). The climate response to stratospheric aerosol geoengineering can be tailored using multiple injection locations. *Journal of Geophysical Research: Atmospheres*, *122*, 12,574–12,590. https://doi.org/10.1002/2017JD026868

Meinshausen, M., Smith, S. J., Calvin, K., Daniel, J. S., Kainuma, M. L., Lamarque, J., et al. (2011). The RCP greenhouse gas concentrations and their extensions from 1765 to 2300. *Climatic Change*, *109*(1), 213–241. https://doi.org/10.1007/s10584-011-0156-z

Mills, M. J., Richter, J. H., Tilmes, S., Kravitz, B., MacMartin, D. G., Glanville, A. A., et al. (2017). Radiative and chemical response to interactive stratospheric sulfate aerosols in fully coupled CESM1(WACCM). *Journal of Geophysical Research: Atmospheres*, *122*, 13,061–13,078. https://doi.org/10.1002/2017JD027006

Mills, M. J., Schmidt, A., Easter, R., Solomon, S., Kinnison, D. E., Ghan, S. J., et al. (2016). Global volcanic aerosol properties derived from emissions, 1990–2014, using CESM1(WACCM). *Journal of Geophysical Research: Atmospheres*, *121*, 2332–2348. https://doi.org/10.1002/2015JD024290

Mote, P. W., Dunkerton, T. J., McIntyre, M. E., Ray, E. A., Haynes, P. H., & Russell, J. M. (1998). Vertical velocity, vertical diffusion, and dilution by midlatitude air in the tropical lower stratosphere. *Journal of Geophysical Research*, *103*(D8), 8651–8666. https://doi.org/10.1029/98JD00203

National Research Council (2015). *Climate intervention: Reflecting sunlight to cool Earth*. Washington, DC: The National Academies Press. https://doi.org/10.17226/18988

Neale, R. B., Chen, C.-C., Gettelman, A., Lauritzen, P. H., Park, S., Williamson, D. L., et al. (2012). Description of the NCAR Community Atmosphere Model (CAM 5.0)., NCAR Technical Note, NCAR TN(486).

Neelin, J. D., Langenbrunner, B., Meyerson, J. E., Hall, A., & Berg, N. (2013). California winter precipitation change under global warming in the Coupled Model Intercomparison Project phase 5 ensemble. *Journal of Climate*, *26*(17), 6238–6256. https://doi.org/10.1175/JCLI-D-12-00514.1

Niemeier, U., & Schmidt, H. (2017). Changing transport processes in the stratosphere by radiative heating of sulfate aerosols. *Atmospheric Chemistry and Physics Discussions*, 1–24. https://doi.org/10.5194/acp-2017-470

Pitari, G., Aquila, V., Kravitz, B., Robock, A., Watanabe, S., Cionni, I., et al. (2014). Stratospheric ozone response to sulfate geoengineering: Results from the Geoengineering Model Intercomparison Project (GeoMIP). *Journal of Geophysical Research: Atmospheres*, *119*, 2629–2653. https://doi.org/10.1002/2013JD020566

Plumb, R. A. (1996). A tropical pipe model of stratospheric transport. *Journal of Geophysical Research*, *101*(D2), 3957–3972. https://doi.org/10.1029/95JD03002

Polvani, L. M., & Kushner, P. J. (2002). Tropospheric response to stratospheric perturbations in a relatively simple general circulation model. *Geophysical Research Letters*, *29*(7), 1114. https://doi.org/10.1029/2001GL014284

Polvani, L. M., Sun, L., Butler, A. H., Richter, J. H., & Deser, C. (2017). Distinguishing stratospheric sudden warmings from ENSO as key drivers of wintertime climate variability over the North Atlantic and Eurasia. *Journal of Climate*, *30*(6), 1959–1969. https://doi.org/10.1175/JCLI-D-16-0277.1

Rasch, P. J., Crutzen, P. J., & Coleman, D. B. (2008). Exploring the geoengineering of climate using stratospheric sulfate aerosols: The role of particle size. *Geophysical Research Letters*, *35*, L02809. https://doi.org/10. 1029/2007GL032179

Richter, J. H., Sassi, F., & Garcia, R. R. (2010). Toward a physically based gravity wave source parameterization in a general circulation model. *Journal of the Atmospheric Sciences*, *67*, 136–156. https://doi.org/10.1175/2009JAS3112.1

Richter, J. H., Tilmes, S., Mills, M. J., Tribbia, J. J., Kravitz, B., MacMartin, D. G., et al. (2017). Stratospheric dynamical response and ozone feedbacks in the presence of SO_2 injections. *Journal of Geophysical Research: Atmospheres*, *122*, 12,557–12,573. https://doi.org/10.1002/2017JD026912

Schirber, S., Manzini, E., Krismer, T., & Giorgetta, M. (2015). The quasi-biennial oscillation in a warmer climate: Sensitivity to different gravity wave parameterizations. *Climate Dynamics*, *45*, 825–836. https://doi.org/10.1007/s00382-014-2314-2

Schmidt, H., Alterskjær, K., Alterskjær, K., Bou Karam, D., Boucher, O., Jones, A., et al. (2012). Solar irradiance reduction to counteract radiative forcing from a quadrupling of CO_2: Climate responses simulated by four Earth system models. *Earth System Dynamics*, *3*(1), 63–78. https://doi.org/10.5194/esd-3-63-2012

Simpson, I. R., Blackburn, M., & Haigh, J. D. (2009). The role of eddies in driving the tropospheric response to stratospheric heating perturbations. *Journal of the Atmospheric Sciences*, *66*(5), 1347–1365. https://doi.org/10.1175/2008JAS2758.1

Simpson, I. R., Shaw, T. A., & Seager, R. (2014). A diagnosis of the seasonally and longitudinally varying midlatitude circulation response to global warming. *Journal of the Atmospheric Sciences*, *71*(7), 2489–2515. https://doi.org/10.1175/JAS-D-13-0325.1

Solomon, S., Rosenlof, K. H., Portmann, R. W., Daniel, J. S., Davis, S. M., Sanford, T. J., & Plattner, G.-K. (2010). Contributions of stratospheric water vapor to decadal changes in the rate of global warming. *Science*, *327*(5970), 1219–1223. https://doi.org/10.1126/science.1182488

Stenchikov, G., Robock, A., Ramaswamy, V., Schwarzkopf, M. D., Hamilton, K., & Ramachandran, S. (2002). Arctic oscillation response to the 1991 Mount Pinatubo eruption: Effects of volcanic aerosols and ozone depletion. *Journal of Geophysical Research*, *107*(24), 4803. https://doi.org/10.1029/2002JD002090

Tilmes, S., Fasullo, J., Lamarque, J. F., Marsh, D. R., Mills, M., Alterskjaer, K., et al. (2013). The hydrological impact of geoengineering in the Geoengineering Model Intercomparison Project (GeoMIP). *Journal of Geophysical Research: Atmospheres*, *118*, 11,036–11,058. https://doi.org/10.1002/jgrd.50868

Tilmes, S., Garcia, R. R., Kinnison, D. E., Gettelman, A., & Rasch, P. J. (2009). Impact of geoengineered aerosols on the troposphere and stratosphere. *Journal of Geophysical Research*, *114*, D12305. https://doi.org/10.1029/2008JD011420

Tilmes, S., Kinnison, D. E., Garcia, R. R., Salawitch, R., Canty, T., Lee-Taylor, J., et al. (2012). Impact of very short-lived halogens on stratospheric ozone abundance and UV radiation in a geo-engineered atmosphere. *Atmospheric Chemistry and Physics*, *12*(22), 10,945–10,955. https://doi.org/10.5194/acp-12-10945-2012

Tilmes, S., Richter, J. H., Mills, M. J., Kravitz, B., MacMartin, D. G., Vitt, F., et al. (2017). Sensitivity of aerosol distribution and climate response to stratospheric SO_2 injection locations. *Journal of Geophysical Research: Atmospheres*, *122*, 12,591–12,615. https://doi.org/10.1002/2017JD026888

Tilmes, S., Richter, J. H., Mills, M. J., Kravitz, B., Macmartin, D. G., Garcia, R. R., et al. (2018). Effects of different stratospheric SO_2 injection altitudes on stratospheric chemistry and dynamics. *Journal of Geophysical Research: Atmospheres*, *123*. https://doi.org/10.1002/2017JD028146

Trepte, C. R., & Hitchman, M. H. (1992). Tropical stratospheric circulation deduced from satellite aerosol data. *Nature*, *355*, 626–628. https://doi.org/10.1038/355626a0

Watanabe, S., & Kawatani, Y. (2012). Sensitivity of the QBO to mean tropical upwelling under a changing climate simulated with an Earth System Model. *Journal of the Meteorological Society of Japan*, *90A*, 351–360. https://doi.org/10.2151/jmsj.2012-A20

Wittman, M. A. H., Charlton, A. J., & Polvani, L. M. (2007). The effect of lower stratospheric shear on baroclinic instability. *Journal of the Atmospheric Sciences*, *64*(2), 479–496. https://doi.org/10.1175/JAS3828.1

Woollings, T., & Blackburn, M. (2012). The north Atlantic jet stream under climate change and its relation to the NAO and EA patterns. *Journal of Climate*, *25*(3), 886–902. https://doi.org/10.1175/JCLI-D-11-00087.1

World Meteorological Organization (1957). Meteorology — A three-dimensional science. *WMO Bulletin*, *6*, 134–138.

Zappa, G., Hoskins, B. J., & Shepherd, T. G. (2015). Improving climate change detection through optimal seasonal averaging: The case of the North Atlantic jet and European precipitation. *Journal of Climate*, *28*(16), 6381–6397. https://doi.org/10.1175/JCLI-D-14-00823.1

Ziemke, J. R., Chandra, S., Labow, G. J., Bhartia, P. K., Froidevaux, L., & Witte, J. C. (2011). A global climatology of tropospheric and stratospheric ozone derived from Aura OMI and MLS measurements. *Atmospheric Chemistry and Physics*, *11*(17), 9237–9251. https://doi.org/10.5194/acp-11-9237-2011